PROCEEDINGS A

rspa.royalsocietypublishing.org

Research

Article submitted to journal

Subject Areas:
condensed matter, statistical mechanics, crystallography

Keywords:
material structure, disorder, diffraction patterns

Author for correspondence:
J. P. Crutchfield
e-mail: chaos@ucdavis.edu

Diffraction Patterns of Layered Close-packed Structures from Hidden Markov Models

P. M. Riechers, D. P. Varn, and J. P. Crutchfield

Complexity Sciences Center & Physics Department, University of California, One Shields Avenue, Davis, California 95616, USA

We develop a method to calculate the diffraction pattern for layered close-packed structures stacked according to the wide class of processes expressible as hidden Markov models. We show that in the limit of large crystals, the diffraction pattern is a particularly simple function of parameters that specify the hidden Markov model. We give three elementary but important examples that demonstrate this result, deriving expressions for the diffraction pattern of close-packed structures stacked: (i) independently, (ii) as infinite-Markov-order randomly faulted 2H and 3C specimens for the entire range of growth and deformation faulting probabilities, and (iii) as a hidden Markov model that describes Shockley-Frank stacking faults in 6H-SiC. We show that the eigenvalues of the transition matrix—as defined by the hidden Markov model—organize and structure the diffraction pattern. Important features of the diffraction pattern are thus severely constrained by the form of the hidden Markov model. To illuminate this connection, we introduce a new visualization technique, the *coronal spectrogram*, that makes explicit the tight relationship between the eigenvalues and the diffraction pattern.

While applied here to planar faulting in close-packed structures, these methods extend in a straightforward way to planar disorder in other layered materials. In this way, we effectively solve the broad problem of calculating a diffraction pattern—either analytically or numerically—for any layered close-packed stacking structure—ordered or disordered—where the stacking process can be expressed as a hidden Markov model.

THE ROYAL SOCIETY PUBLISHING

1. Introduction

Since the fundamental forces that bind materials are isotropic, it may be surprising that so many materials have such strongly anisotropic structures. That is, the bonds may not be of equal strength in all directions, instead showing relatively strong preferential bonding in two of the directions, with much weaker interactions along a third direction. We say that the resulting material is *layer-like* with strong *intralayer* bonding and weaker *interlayer* bonding. Other mechanisms may contribute to a material having a layer-like structure. For example, some form as a result of a layer-by-layer growth process; and, of course, it is now possible to engineer artificially layered materials with great precision [1,2]. These various mechanisms conspire to create a great variety of materials that are conveniently thought of as being composed of stacked layers. Examples are numerous: micas such as muscovite and phlogopite [3]; III-V compounds such as GaS and InSe [4], which are of interest due their electronic and optical properties; SiC and ZnS [4], which are known to have hundreds of stable crystalline structures resulting from their layer-like properties; perovskites such as $BaRuO_3$ and $CaTiO_3$ [5]; graphene and hexagonal BN [1], which have attracted great interest for their electronic properties; and lastly, metal dichalcogenides such as MoS_2 and WSe_2 [6].

Although restricted to a few alternatives, often there is more than one way to stack two adjacent layers, and much of the interesting physics and crystallography occurs as one traverses a material perpendicular to these layers in what is called the *stacking direction* [7]. One such phenomenon is *polytypism* [8], where a material built up of identical layers can coexist in two or more stable crystalline stacking configurations. SiC in particular is known to have hundreds of such periodic (and hence crystalline) stacking configurations, some with periodicities extending over one hundred layers [4]. Given the weak layer-to-layer interactions in many of these materials as well as the small energy differences between some stacking sequences, they are prone to errors in the stacking configuration called *stacking faults* [9,10]. These deviations from periodic stacking can occur during the growth process or through some post-formation stress to the specimen, be it mechanical, thermal, or irradiative [4]. The resulting specimen is disordered, sometimes even to the point of losing any meaningful sense of an underlying periodic stacking structure [11,12]. While these planar defects have, of course, been known and studied for some time they have often been viewed as a nuisance or feature to be minimized or eliminated [13]. Increasingly though, materials scientists are appreciating the sometimes unexpected role that disorder and crystal defects play in material properties. For example, disordered graphene nanosheets can be used to improve the performance of high-capacity Li ion batteries [14], and so-called 'defect engineering' in semiconductors is attracting wide attention [15].

Given the growing technological import of disordered materials, methods of detecting experimentally and then describing the resulting structures are needed. Since its discovery in the early 20th century, X-ray diffraction has proved invaluable for determining material structure, for both ordered and disordered materials [16]. Typically in a diffraction experiment, one uses a probe, most often a finely collimated beam of monochromatic X-rays, electrons, or neutrons focused on the specimen at some angle and subsequently one collects the diffracted reflections. When this is performed over a variety of angles, one generates a *diffraction pattern*.[1] While many physical effects can influence the diffraction pattern [18], most can be corrected for and the diffraction pattern is profitably viewed as the power spectrum of the real space arrangement of atoms. Thus, the diffraction pattern is highly sensitive to material structure and diffraction experiments remain the workhorse of modern material structure determination.

It is also important to efficiently, compactly, and consistently describe such disordered layered materials. *Classical crystallography*, based on the geometric symmetries found in perfectly crystalline materials and couched in the language of finite group theory, has enjoyed enormous

[1]Common geometries and techniques for diffraction experiments, particularly X-ray diffraction, can be found in any text on condensed matter physics, such as Ashcroft & Mermin [17], or any crystallographic text such as Giacovazza *et al.* [18], Warren [19], and Guinier [20].

success. However, there has long been a call to expand the range of classical crystallography to treat other structures, particularly those that are not perfectly ordered [21,22]. Indeed, classical crystallography has not proved nearly as useful when characterizing materials that show disorder, especially if that disorder is profound. To circumvent these limitations, a new perspective on the structure of materials has recently been proposed. *Chaotic crystallography* is the application of information- and computation-theoretic methods to the discovery and description of disorder in materials [7,23]. Drawing from concepts developed in information theory [24], theoretical computer science [25,26] and nonlinear dynamics [27], chaotic crystallography adapts and applies *computational mechanics* [28,29] to the problem of disorder in materials. Instead of relying on exact geometric symmetries, chaotic crystallography captures structure in terms of partial and noisy symmetries, formulated in the language of semi-groups. Setting order and disorder on equal footing, chaotic crystallography provides novel platform to understand material structure.

Quasi-one-dimensional materials are particularly amenable to analysis by the methods of chaotic crystallography. One scans the specimen along the stacking direction recording the kind and orientation of the layers as they are encountered, assigning a symbol to each of the possible kinds and orientations. The resulting list of symbols is called the *stacking sequence* [30], and the effective stochastic process induced is called the *stacking process* [30]. Sequential symbolic data such as this have been well-studied in the physical sciences and are sometimes analyzed using *hidden Markov models* [31,32]. A rich set of analytical tools has been developed to study hidden Markov models, and here we will augment that toolset by demonstrating how the diffraction pattern can be directly calculated from an arbitrary hidden Markov model, either efficiently to great numerical accuracy or analytically.

We report two major advances. (i) Although the problem of connecting disordered stacking structures to diffraction patterns has been addressed by many previous authors, we offer a new derivation of an expression to calculate the diffracted intensity of close-packed layered materials in terms of the hidden Markov model that describes the stacking process. This is carried out by explicitly treating either ordered or disordered stacking configurations as an arbitrary hidden Markov model, which to our knowledge has not been previously done. (ii) Spectral analysis of the hidden Markov model will lead us to a new way to visualize diffraction patterns for layered materials, in what we call *coronal spectrograms*. We will introduce these versatile and informative graphs in §5, where we will find that they result in significant insights into stacking structures.

Our development is organized as follows: §2 reviews historical milestones in the study of diffraction patterns from layered materials and familiarizes the reader with modeling stochastic processes; §3 fixes nomenclature and definitions; §4 derives a general expression for the diffraction pattern of layered close-packed structures in terms of an arbitrary hidden Markov model; §5 introduces coronal spectrograms and considers several examples, namely (i) an independently distributed process that can model 3C or random stacking structures, (ii) an infinite-order-Markov stacking process that represents any amount of random growth and deformation faults in 3C and 2H structures, and (iii) a stacking process inspired by recent experiments in 6H-SiC; and §6 gives our conclusions and outlines directions for future work.

2. Background

(a) Brief History of Planar Disorder and Diffraction Patterns

There is a long history of researchers treating the problem of calculating diffraction patterns from layered materials and the interested reader is encouraged to consult Treacy *et al.* [33] for a thorough and detailed treatment or Estevez-Rams [34] for a shorter but more recent exposition.

Landau [35] and Liftshitz [36] are usually credited as the first to treat the problem, when in 1937 they considered the effect of stacking disorder, assuming no correlation among the stacking defects. In 1942 Hendricks & Teller [37] developed the *matrix formalism method*, where a transition matrix specifies the probability of observing a layer, possibly dependent on a previous history

of observed layers. They considered four cases: (i) no interaction between layers with each layer having the same form factor, (ii) randomly distributed layers having variable spacing, (iii) the probabilities of the occurrence of layers depending on the nearest neighbors, and (iv) the probabilities of occurrence of layers depending on nearest and next nearest neighbors. Also in 1942 Wilson [38] examined the case of hexagonal closed-packed Co with randomly distributed planar faults, pioneering the *difference equation method*. Jagodzinski [39,40] in 1949 introduced the *reichweite*, denoted s, that allows variable range of influence between layers in close-packed structures. He found solutions for small s, but noted that the calculations become onerous for $s > 3$. In 1986 Berliner & Werner [41] demonstrated that the diffraction pattern for a specific stacking sequence can be calculated directly by *Monte Carlo* or *crystal growth methods*, where one simulates a crystal by 'growing' it according to some rules, and then sums the contributions to the reflected wave for all layers in the sample. They applied this technique to growth and deformation faults in Li and compared the results with experimental neutron diffraction studies. Many other researchers have expanded on these methods, leaving an extensive literature [33,34,42].

However, most relevant to the development we pursue here is the 1991 seminal work by Treacy *et al.* [33]. They offered a *general recursion matrix method* to calculate the diffraction pattern for layered materials, implementing it in a freely available and well-used computer software package called *DIFFaX*. Key to their approach is the recognition that by a judicious grouping of terms it is possible to perform analytically the sum over layers to calculate the diffraction pattern. As part of their procedure, they assume a transition matrix that gives the probabilities of transitioning to any other layer, given the current layer.

To place our contributions in context of these previous efforts, it is necessary to discuss how these models can be classified according to their computational-theoretic capabilities. In the next section we offer a tour of the differences between the kinds of models that have been used and in §3(b) we give a mathematically grounded treatment of the stacking process as generated by a hidden Markov model.

(b) Markov Models and Hidden Markov Models

Let us consider models that are capable of probabilistically generating a sequence of symbols, where the symbols are taken from some finite set. Important distinctions between different models rest on how they condition the probability of observing a current symbol on a previously observed, perhaps even infinite, history of symbols. The simplest assumption is that the current symbol in the sequence takes its particular value independent of all the other symbols in the sequence. If, further, the probability distribution over symbols is invariant to a shift in sequence position, the model is called *independent and identically distributed* (IID). By definition, these models admit no correlation between symbols.

The next level of complication occurs when we allow the value of the current symbol to depend on the previous symbol, and *only* the previous symbol. These models are called Markov models (MMs). Since it is only the value of the previous symbol that is needed to give the best prediction of the current symbol, it is possible to label the states of the MM by the current symbol. Trivially, then, one knows the sequence of states by the observed symbol sequence, since they are identical. Concomitantly, for MMs, the total number of states of the model is strictly limited by the number of the kinds of symbols observed.

An additional complication occurs when it is necessary to know not only the previous symbol, but a finite history of previous symbols. These *finite-order Markov models* (fMMs) are often further specified by the length of the history needed, sometimes denoted r [43], and are called rth-order Markov models. For $r = 1$, fMMs degenerate to the MMs considered earlier, and if we allow the case that $r = 0$, then zeroth-order Markov models generate the IID processes. Note that for $r \geq 2$ it is no longer possible to label the states by the observed symbol. In this sense, the states of the model become *hidden*, as the sequence of states is no longer just the observed sequence of symbols.

Perhaps surprisingly, often the next symbol in a sequence depends on an infinite history of symbols. This is best explained by giving an example. Suppose that a sequence composed of only

0s and 1s conforms to the following rule: one can observe a consecutive sequence of 1s of any length; however, between any two 1s there must be an *even* number of 0s. Thus, on observing a 0, one also needs to know the symbol preceding it. If that symbol were 1, such that the two-symbol history was 10, then to retain the evenness of 0s the next symbol would perforce be 0. If it was not, then we would have the sequence 101, which is not allowed. Indeed, it becomes apparent that when one observes a consecutive sequence of 0s, it is important to keep track of whether there has been an even or odd number of them. Since this history could extend back indefinitely, this process, called the *even process* [44,45], entails a special kind of infinite memory. Nonetheless, it is possible to describe this process by using only two states: (a) if the history of symbols ends in 1 or an even number of consecutive 0s, then the next symbol is either 0 or 1; (b) if the history is an odd number of 0s, then the next symbol is 0. Borrowing terminology from the computation theory of formal languages, the even process is an example of a *strictly sofic process* [44,45] and has been treated in the context of close-packed layered materials elsewhere [43]. Models such as the even process that remember an infinite past with a finite memory (using a finite number of states) are called *infinite-order Markov models* (iMMs).

For IIDs, MMs, and fMMs, if the system is in a particular state and makes a transition to another state, the symbol observed on this transition uniquely determines the successor state. This property is called *unifilarity* [46]. If this condition is relaxed so that the state and the observed symbol are not sufficient to determine the next state, these models are *nonunifilar*. This distinction becomes important for infinite-order Markov models, and those with unifilarity are called *unifilar infinite-order Markov models* (uiMMs) and those without it are called *nonunifilar infinite-order Markov models* (niMMs). From the development, it should be apparent that these models are hierarchically related, such that models lower on the hierarchy are special cases of those above it.[2] The model-class hierarchy is:

$$\text{IID} \subset \text{MM} \subset \text{fMM} \subset \text{uiMM} \subset \text{niMM} \,. \tag{2.1}$$

Let us revisit previous models of disorder and classify them by their place on the hierarchy. Landau [35], Liftshitz [36], and the first two cases of Hendricks & Teller [37] are IID models. Hendricks & Teller's third case, where the probabilities only depend on the single preceding layer, are MMs. Finally, by grouping layers, Hendricks & Teller were able to effectively construct a 2nd-order MM (*i.e.*, a fMM) in their last case. Similarly, a careful treatment of the model proposed by Wilson [38] shows that it is a 2nd-order MM, as he conditions the fault probability on the values of the previous two layers.[3] Jagodzinski's reichweite [39,40] is clearly related to the Markov order. If one writes the stacking sequence in the HK-notation [4,49], then $s = 3$ can be expressed as a MM and $s = 4$ as a 2nd-order MM. The Monte Carlo method of Berliner & Werner [41] is not a distinct model class in the same sense that the others are, since there is no 'compactification' of the rules governing the stacking process. By explicit calculation from a particular stacking sequence, it can effectively calculate the diffraction pattern for any of the models in Eq. (2.1). ϵ-Machine spectral reconstruction theory [30,43,50,51], an alternative sequence-based estimation method, has been implemented up to 3rd-order MMs, although in previous applications it used the Monte Carlo method to calculate diffraction patterns. Lastly, the recursion matrix method of Treacy *et al.* [33] explicitly treats MMs, although by grouping layers as proposed by Hendricks & Teller, it can treat fMMs.

It should be noted that the Monte Carlo method, though now in common usage, is not altogether satisfactory. One difficulty lies in the statistical fluctuations inherent in the finite-size samples it uses. It is known that these lead to estimation errors in the power spectrum on the order of the magnitude of the power spectrum itself [52]. This difficulty can be ameliorated by taking many samples and averaging [53] or by using a smoothing procedure [51]. A second concern arises when repeated comparison of calculated and experimental diffraction patterns is needed

[2] For a full discussion, see Crutchfield [47] and Crutchfield & Marzen [48].

[3] There is a subtlety here. Wilson defines his model in terms of the ABC-notation of the close-packed layers. By rewriting the stacking sequence in a different nomenclature, it is possible to recast his model as a 1st-order MM or even simply a MM. This particular model, as well as the dependence of the Markov order on the notation used, is treated in detail elsewhere [12].

for inference procedures such as reverse Monte Carlo modeling [54] and differential evolution and genetic algorithms [55]. For samples of reasonable size, the Monte Carlo method is clearly much less efficient than the matrix formalism or difference equation methods.

It might be thought that the description of stacked layers would not require such sophisticated models. However, especially when a layered specimen is undergoing solid-state transformation, such as by annealing, effectively infinite-range memories can be induced [56]. As the layers shift, energetic considerations can restrict the number of paths to disorder, leaving a remnant of the crystalline stacking structure imprinted in the disordered specimen. Equilibrium is often not obtained, and the structure finds itself caught in a local minimum of the free energy, lacking the necessary activation energy to explore all of phase space. In addition to their expected importance, neglecting infinite-order Markov models in favor of only finite-order Markov models severely restricts the space of possible models considered. James *et al.* [57] showed that as a function of the number of states, the number of topologically distinct finite-order MMs is dwarfed as compared to the number of distinct infinite-order MMs. For six-state processes, a full 98% of the models were infinite-order Markov. Thus, models capable of capturing infinite-range memory are needed.

To our knowledge, no method has yet been shown to calculate diffraction patterns of infinite-order Markov models (uiMMs or niMMs) either analytically or in closed form. In the following, we offer a general, analytical solution to this problem for stacking processes in close-packed structures describable as a hidden Markov model.

3. Definitions and Notations

We will confine our exposition to close-packed structures (CPSs). For many materials, such as SiC, CdI_2, and GeSe [4], there may be several layers of atoms that act as a unit and it is these units which obey the close-packing rules. We will refer to these units as *modular layers* (MLs) [58, 59]. Let us make the following assumptions concerning the stacking of MLs in CPSs: (i) the MLs themselves are undefected and free of any distortions; (ii) the spacing between MLs does not depend on the local stacking arrangement; (iii) each ML has the same scattering power; and (iv) the faults extend laterally completely across the crystal.

Additionally, we assume that the unconditioned probability of finding a given stacking sequence remains constant through the crystal. (In statistics parlance, we assume that the stacking process is *weak-sense stationary*. Physically, the process is spatial-translation invariant.)

(a) Correlation Functions and Stacking Notation

In CPSs, each ML may assume one of three possible orientations, usually labeled A, B, and C [17].We say that two MLs in a sequence are *cyclically* related if the ML further along in the sequence can be obtained from the earlier ML via a cyclic permutation (*i.e.*, $A \to B \to C \to A$), and *anticyclically* related if it can be obtained via an anticyclic permutation (*i.e.*, $A \to C \to B \to A$). It is convenient to introduce three statistical quantities [51], $Q_{\mathrm{c}}(n)$, $Q_{\mathrm{a}}(n)$, and $Q_{\mathrm{s}}(n)$: the pairwise (auto)correlation functions (CFs) between MLs that are the probability any two MLs at separation n are related cyclically (c), anticyclically (a), or have the same orientation (s), respectively. It is also useful to introduce a family of cyclic-relation functions [60] $\hat{\xi}(x) \in \{\hat{\mathrm{c}}(x), \hat{\mathrm{a}}(x), \hat{\mathrm{s}}(x)\}$, where, for example:

$$\hat{\mathrm{c}}(x) = \begin{cases} B & \text{if } x = A \\ C & \text{if } x = B \\ A & \text{if } x = C \end{cases} . \tag{3.1}$$

The other two operators, $\hat{\mathrm{a}}(x)$ and $\hat{\mathrm{s}}(x)$, are defined in an obviously analogous fashion.

It is sometimes advantageous to exploit the constraint that no two adjacent MLs may occupy the same orientation in CPSs. Thus, we sometimes use the Hägg-notation, where cyclic transitions between adjacent MLs are denoted with '+', and anticyclic ones with '-'. (Ortiz *et al.* [49] give an excellent treatment of the various notations used to describe CPSs.) Often it is more convenient to

substitute '1' for '+' and '0' for '-' and we make this substitution throughout. The two notations, the Hägg-notation and the ABC-notation, carry an equivalent message (up to an overall rotation of the specimen about the stacking direction), albeit in different tongues.

(b) The Stacking Process as a Hidden Markov Model

Previously, it was shown that the stacking process for many cases of practical interest can be written as a discrete-step, discrete-state hidden Markov model (HMM) [60], and we review notations and conventions now.

We assume that the statistics of the stacking process are known and can be expressed as a HMM in the form of an ordered tuple $\Gamma = (\mathcal{A}, \mathbb{S}, \mu_0, \mathbf{T})$, where $\mathcal{A}$ is a set of symbols output by the process and often called an *alphabet*, $\mathbb{S}$ is a finite set of M internal (and possibly hidden) states, μ_0 is an initial state probability distribution, and $\mathbf{T}$ is a set of $|\mathcal{A}|$ M-by-M transition matrices (TMs) that give the transition probabilities between states on emission of one of the symbols in $\mathcal{A}$.

For the CPSs, the output symbols are just ML orientations and, thus, this alphabet can either be written in the Hägg-notation or the ABC-notation. Since the latter is more convenient for our purposes, we take $\mathcal{A} = \mathcal{A}_{\mathrm{P}} \equiv \{A, B, C\}$. $\mathbb{S}$ is the set of M states that comprise the process; *i.e.*, $\mathbb{S} = \{\mathcal{S}_1, \mathcal{S}_2, \ldots, \mathcal{S}_M\}$. Lastly, there is one $M \times M$ TM for each output symbol, so that $\mathbf{T} = \{\mathcal{T}^{[A]}, \mathcal{T}^{[B]}, \mathcal{T}^{[C]}\}$. These emission-labeled transition probability matrices are of the form:

$$\mathcal{T}^{[x]} = \begin{bmatrix} \Pr(x, \mathcal{S}_1|\mathcal{S}_1) & \Pr(x, \mathcal{S}_2|\mathcal{S}_1) & \cdots & \Pr(x, \mathcal{S}_M|\mathcal{S}_1) \\ \Pr(x, \mathcal{S}_1|\mathcal{S}_2) & \Pr(x, \mathcal{S}_2|\mathcal{S}_2) & \cdots & \Pr(x, \mathcal{S}_M|\mathcal{S}_2) \\ \vdots & \vdots & \ddots & \vdots \\ \Pr(x, \mathcal{S}_1|\mathcal{S}_M) & \Pr(x, \mathcal{S}_2|\mathcal{S}_M) & \cdots & \Pr(x, \mathcal{S}_M|\mathcal{S}_M) \end{bmatrix},$$

where $x \in \mathcal{A}_{\mathrm{P}}$ and $\mathcal{S}_1, \mathcal{S}_2, \ldots, \mathcal{S}_M \in \mathbb{S}$.

It is often useful to have the total state-to-state TM, whose components are the probability of transitions independent of the output symbol, and it is given by the row-stochastic matrix $\mathcal{T} = \mathcal{T}^{[A]} + \mathcal{T}^{[B]} + \mathcal{T}^{[C]}$. There also exists a stationary distribution $\boldsymbol{\pi} = \big(\Pr(\mathcal{S}_1), \ldots, \Pr(\mathcal{S}_M)\big)$ over the hidden states, such that $\langle\boldsymbol{\pi}| = \langle\boldsymbol{\pi}|\,\mathcal{T}$. We make limited use of a bra-ket notation throughout the following, where bras $\langle\cdot|$ represent row vectors and kets $|\cdot\rangle$ represent column vectors. Bra-ket closures, $\langle\cdot\rangle$ or $\langle\cdot|\cdot\rangle$, are scalars and commute as a unit with anything.

In the Hägg representation, the state-to-state transition matrix is $\mathsf{T} = \mathsf{T}^{[0]} + \mathsf{T}^{[1]}$. In that case the stationary distribution $\boldsymbol{\pi}_{\mathrm{H}}$ can be obtained from $\langle\boldsymbol{\pi}_{\mathrm{H}}| = \langle\boldsymbol{\pi}_{\mathrm{H}}|\,\mathsf{T}$.

HMMs are often depicted as labeled directed graphs called probabilistic finite-state automata (FSA) [25,26]. When written using the ABC-notation, we refer to such an automaton as the ABC-machine and, similarly, when written in terms of the Hägg-notation, such an automaton is referred to as the Hägg-machine. It is a straightforward task to translate a Hägg-machine into an ABC-machine [60]. For completeness, we reproduce the minimal algorithm in the appendix.

We note that while Hägg-notation and Hägg-machines are useful shorthand, the primary mathematical object for the development here is the ABC-machine, since this describes the stacking process in the natural language of the $\{Q_\xi(n)\}$. It is, however, often easier to give just the Hägg-machine since the expansion procedure is straightforward. Fundamentally, however, it is the ABC sequences that directly relate to structure factors for the specimen. And, this practical consideration is the principle reason for using the ABC-notation and ABC-machines.

(c) Mixing and Nonmixing Machines

When expanding the Hägg-machine into an ABC-machine, two important cases emerge: *mixing* and *nonmixing* Hägg-machines. Which of these two cases we are considering has implications for the resultant DP, and so it is important to distinguish them [60].

In the expansion process, the number of states is tripled to account for the possible degeneracy of the ABC-notation. That is, we require that the ABC-machine keep track of not only the relative

orientation between adjacent MLs (as the Hägg-machine does), but also the absolute A, B, or C orientation. In doing so, we allow a state architecture that can accommodate this increased representation requirement. For *mixing* machines, the resultant FSA is *strongly connected*, such that any state is accessible to any other state in a finite number of transitions. We find that this is by far the more common case. For *nonmixing* machines, the resultant graph is not strongly connected, but instead breaks into three unconnected graphs, each retaining the state structure of the original Hägg-machine. Only one of these graphs is physically realized in any given specimen, and we may arbitrarily choose to treat just one of them. The deciding factor on whether a machine is mixing or nonmixing depends on its architecture: if there exists at least one closed, nonself-intersecting state path that corresponds to an overall rotation of the specimen, then the machine is mixing. The closed path is called a *simple state cycle* (SSC) on a FSA or a *causal state cycle* (CSC) if the FSA is also an ϵ-machine. All of the examples we consider here are mixing machines over most of their parameter range.

(d) Power Spectra

Since we are considering only finite-state HMMs, $\mathcal{T}$ is a finite-dimensional square matrix, and so its spectrum is just its set of eigenvalues:

$$\Lambda_{\mathcal{T}} = \{\lambda \in \mathbb{C} : \det(\lambda \mathbb{I} - \mathcal{T}) = 0\} \ , \tag{3.2}$$

where $\mathbb{I}$ is the $M \times M$ identity matrix. Since $\mathcal{T}$ is row-stochastic (*i.e.*, all rows sum to one), all of its eigenvalues live on or within the unit circle in the complex plane. The connection between the operator's spectrum and the diffraction spectrum will become clear shortly. In brief, though, eigenvalues along the unit circle lead to Bragg peaks; eigenvalues within the unit circle are responsible for diffuse peaks associated with disorder—the diffuse diffraction pattern (DP) is the shadow that these eigen-contributions cast along the unit circle.

In the limit of infinite-length sequences,[4] power spectra generally can be thought of as having three distinct contributions; namely, *pure point* (pp), *absolutely continuous* (ac), and *singular continuous* (sc). Thus, a typical power spectrum $\mathcal{P}(\omega)$ can be decomposed into [45,61]:

$$\mathcal{P}(\omega) = \mathcal{P}_{pp}(\omega) + \mathcal{P}_{ac}(\omega) + \mathcal{P}_{sc}(\omega) \ . \tag{3.3}$$

Pure point spectra are physically realized as Bragg reflections in DPs, and diffuse or broadband scattering is associated with the absolutely continuous part. Singular continuous spectra are not often observed in DPs from quasi-one-dimensional crystals, although specimens can be engineered to have a singular continuous portion in the DP, as for example layered GaAs-AlAs heterostructures stacked according to the Thue-Morse process [62]. Since these more exotic processes are not expressible as finite-state HMMs, we do not consider them further for now.

It might be thought that the more pedestrian forms of disorder in layered materials—such as growth, deformation, or layer-displacement faults—always destroy the long-range periodicity along the stacking direction and, thus, 'true' Bragg reflections need not be treated. (This is in contrast to those cases where there is little disorder and the integrity of the Bragg reflections is largely preserved.) In fact, there are occasions, such as solid-state transformations in materials with competing interactions between MLs [63,64] or those with disordered and degenerate ground states [59,65] that do maintain long-range correlations. Hence, it is not possible to exclude the existence of Bragg reflections *a priori*. Thus, we generally consider both Bragg reflections (B) and diffuse scattering (D) here and write the DP $\mathsf{I}(\ell)$ as having two contributions:

$$\mathsf{I}(\ell) = \mathsf{I}_{\mathrm{B}}(\ell) + \mathsf{I}_{\mathrm{D}}(\ell) \ , \tag{3.4}$$

where $\ell \in \mathbb{R}$ is a continuous variable that indexes the magnitude of the perpendicular component of the diffracted wave: $k = \omega/c = 2\pi\ell/c$ with c being the distance between adjacent MLs of the crystal.

[4]For power spectra of finite-length sequences, there is no clear distinction among these features.

Fortunately, knowledge of the HMM allows us to select beforehand those values of ℓ potentially contributing Bragg reflections. Let $\Lambda_{\rho(\mathcal{T})} \equiv \{\lambda \in \Lambda_{\mathcal{T}} : |\lambda| = 1\}$. The values of ℓ for which $\mathrm{e}^{i2\pi\ell} \in \Lambda_{\rho(\mathcal{T})}$ are the only ones where there may possibly exist Bragg reflections. It is immediately apparent, then, that the total number of Bragg reflections within a unit interval of ℓ in the DP cannot be more than the number M of HMM states. Conversely, the total number of Bragg reflections sets a minimum on M.

4. Diffraction Patterns from Hidden Markov Models

With definitions and notations in place, we now derive our main results: analytical expressions for the DP in terms of the parameters that define a given HMM. We split our treatment into two steps: (i) we first treat the diffuse part of the spectrum and, then, (ii) we treat those z-values ($z \equiv \mathrm{e}^{i\omega} = \mathrm{e}^{i2\pi\ell}$) corresponding to eigenvalues of the TM along the unit circle.

(a) Diffuse Scattering

The corrected DP[5] for CPSs along a row defined by $h_0 - k_0 = 1 \pmod 3$, where h_0, k_0 are components of the reciprocal lattice vectors in the plane of the MLs, can be written as [51,65,66]:

$$\mathsf{I}^{(N)}(\ell) = \frac{\sin^2(N\pi\ell)}{N\sin^2(\pi\ell)} - \frac{2\sqrt{3}}{N}\sum_{n=1}^{N}(N-n)\Big[Q_{\mathrm{c}}(n)\cos\left(2\pi n\ell + \tfrac{\pi}{6}\right) + Q_{\mathrm{a}}(n)\cos\left(2\pi n\ell - \tfrac{\pi}{6}\right)\Big] \quad (4.1)$$

$$= \frac{\sin^2(N\pi\ell)}{N\sin^2(\pi\ell)} - \frac{2\sqrt{3}}{N}\,\Re\left\{\sum_{n=1}^{N}(N-n)\left[Q_{\mathrm{c}}(n)\,\mathrm{e}^{-i2\pi n\ell}\mathrm{e}^{-i\pi/6} + Q_{\mathrm{a}}(n)\,\mathrm{e}^{-i2\pi n\ell}\mathrm{e}^{i\pi/6}\right]\right\} .$$

$Q_{\mathrm{c}}(n)$ and $Q_{\mathrm{a}}(n)$ are the previously defined CFs and N is the total number of MLs in the specimen.[6] The superscript N on $\mathsf{I}^{(N)}(\ell)$ reminds us that this expression for the diffuse DP depends on the number of MLs. The first term in Eq. (4.1) is the Fejér kernel. As the number of MLs becomes infinite, this term will tend to a δ-function at integer values of ℓ, which may be altered or eliminated by δ-function contributions from the summation: an issue we address shortly. It is only the second term, the summation, that results in diffuse scattering even as $N \to \infty$. It has previously been shown [60] that the CFs, in turn, can be written in terms of the labeled and unlabeled TMs of the underlying stacking process as:

$$Q_{\xi}(n) = \sum_{x\in\mathcal{A}_{\mathrm{P}}} \langle\boldsymbol{\pi}|\,\mathcal{T}^{[x]}\mathcal{T}^{n-1}\mathcal{T}^{[\hat{\xi}(x)]}\,|\mathbf{1}\rangle \ , \quad (4.2)$$

where we denote the asymptotic probability distribution over the HMM states as the length-M row vector $\langle\boldsymbol{\pi}|$ and a length-M column vector of 1s as $|\mathbf{1}\rangle$. For mixing processes, Eq. (4.2) simplifies to the more restricted set of equations:

$$Q_{\xi}(n) = 3\,\langle\boldsymbol{\pi}|\,\mathcal{T}^{[x]}\mathcal{T}^{n-1}\mathcal{T}^{[\hat{\xi}(x)]}\,|\mathbf{1}\rangle \ , \ \text{where } x \in \mathcal{A}_{\mathrm{P}} \ . \quad (4.3)$$

[5] As previously done [51], we divide out those factors associated with experimental corrections to the observed DP, as well as the total number N of MLs, so that $\mathsf{I}(\ell)$ has only those contributions arising from the stacking structure itself. Here and elsewhere, we refer to $\mathsf{I}(\ell)$ simply as the DP. Note however that factoring out the structure factors, etc. is not necessary. A more general expression is obtained by retaining these effects in the expression for the diffracted intensity. Note that the treatment by Treacy *et al.* [33] retains these factors.

[6] It may seem that specializing to such a specific expression for the DP at this stage limits the applicability of the approach. While the development here is restricted to the case of CPS, under mild conditions, the Wiener-Khinchin theorem [45] guarantees that power spectra can be written in terms of pair autocorrelation functions, as is done here. This makes the spectral decomposition rather generic.

Thus, we can rewrite the DP directly in terms of the TMs of the underlying stacking process as:

$$\mathsf{I}^{(N)}(\ell) = \frac{\sin^2(N\pi\ell)}{N\sin^2(\pi\ell)} - \frac{2\sqrt{3}}{N}\ \Re\left\{\sum_{x\in\mathcal{A}_\mathrm{P}} \langle\boldsymbol{\pi}|\,\mathcal{T}^{[x]}\left(\sum_{n=1}^{N}(N-n)\,z^{-n}\mathcal{T}^{n-1}\right)\left(\mathrm{e}^{-i\pi/6}\mathcal{T}^{[\hat{\mathrm{c}}(x)]} + \mathrm{e}^{i\pi/6}\mathcal{T}^{[\hat{\mathrm{a}}(x)]}\right)|\mathbf{1}\rangle\right\}, \tag{4.4}$$

where we have introduced the ℓ-dependent variable $z \equiv \mathrm{e}^{i2\pi\ell}$. Furthermore, we can evaluate the summation over n in Eq. (4.4) analytically. First, we note that the summation can be re-indexed and split up as:

$$\sum_{n=1}^{N}(N-n)\,z^{-n}\mathcal{T}^{n-1} = z^{-1}\sum_{\eta=0}^{N-1}(N-1-\eta)\,(\mathcal{T}/z)^{\eta} \tag{4.5}$$

$$= z^{-1}\left\{(N-1)\left[\sum_{\eta=0}^{N-1}(\mathcal{T}/z)^{\eta}\right] - \left[\sum_{\eta=0}^{N-1}\eta\,(\mathcal{T}/z)^{\eta}\right]\right\}. \tag{4.6}$$

For finite positive integer N, it is always true that:

$$(z\mathbb{I}-\mathcal{T})\sum_{\eta=0}^{N-1}(\mathcal{T}/z)^{\eta} = z\left[\mathbb{I}-(\mathcal{T}/z)^{N}\right] \tag{4.7}$$

and

$$(z\mathbb{I}-\mathcal{T})\sum_{\eta=0}^{N-1}\eta\,(\mathcal{T}/z)^{\eta} = z\left\{\left[\sum_{\eta=0}^{N-1}(\mathcal{T}/z)^{\eta}\right] - N(\mathcal{T}/z)^{N} - \left[\mathbb{I}-(\mathcal{T}/z)^{N}\right]\right\}. \tag{4.8}$$

Hence, for $z \notin \Lambda_{\mathcal{T}}$, $z\mathbb{I}-\mathcal{T}$ is invertible and we have:

$$\sum_{n=1}^{N}(N-n)\,z^{-n}\mathcal{T}^{n-1} = (z\mathbb{I}-\mathcal{T})^{-1}\left\{N\mathbb{I} - z(z\mathbb{I}-\mathcal{T})^{-1}\left[\mathbb{I}-(\mathcal{T}/z)^{N}\right]\right\}. \tag{4.9}$$

Putting this all together, we find the expected value of the finite-N DP for all $z = \mathrm{e}^{i2\pi\ell} \notin \Lambda_{\mathcal{T}}$:

$$\mathsf{I}^{(N)}(\ell) = \frac{\sin^2(N\pi\ell)}{N\sin^2(\pi\ell)} - 2\sqrt{3}\ \Re\left\{\sum_{x\in\mathcal{A}_\mathrm{P}} \langle\boldsymbol{\pi}|\,\mathcal{T}^{[x]}(z\mathbb{I}-\mathcal{T})^{-1}\left\{\mathbb{I} - \frac{z}{N}(z\mathbb{I}-\mathcal{T})^{-1}\left[\mathbb{I}-(\mathcal{T}/z)^{N}\right]\right\}\right.$$
$$\left.\times\left(\mathrm{e}^{-i\pi/6}\mathcal{T}^{[\hat{\mathrm{c}}(x)]} + \mathrm{e}^{i\pi/6}\mathcal{T}^{[\hat{\mathrm{a}}(x)]}\right)|\mathbf{1}\rangle\right\}, \tag{4.10}$$

with $z \equiv e^{i2\pi\ell}$. This gives the most general relationship between the DP and the TMs of the underlying stacking process. We see that the effects of finite crystal size come into the diffuse DP via a $1/N$-decaying term containing the N^{th} power of both z^{-1} and the unlabeled TM. This powerful result directly links the stacking process rules to the observed DP and, additionally, already includes the effects of finite specimen size.

Eq. (4.10) should be compared with Eqs. (16) and (17) of Treacy *et al.* [33]. Note the similar form, especially that the *resolvent* [67], $(z\mathbb{I}-\mathcal{T})^{-1}$, finds an analog in the term $(I-T)^{-1}$ of Eq. (16) of Treacy *et al.* However our result is obtained by assuming a HMM that describes the stacking process, and not a judicious grouping of terms as has been done previously [33]. Whether the results of Treacy *et al.* are sufficiently general to include infinite-order Markov models, or can be modified to do so, remains an open question.

For many cases of practical interest, the specimen can be treated as effectively infinite along the stacking direction. (In follow-on work, we explore the effects of finite specimen size.) In this

limiting case, the relationship between the diffuse DP and the TMs becomes especially simple. In particular, as $N \to \infty$ the DP's diffuse part becomes:

$$\mathsf{I}_{\mathrm{D}}(\ell) = \lim_{N\to\infty} \mathsf{I}^{(N)}(\ell) = -2\sqrt{3}\ \Re\left\{ \sum_{x\in\mathcal{A}_{\mathrm{P}}} \langle \boldsymbol{\pi}|\, \mathcal{T}^{[x]}\, (z\mathbb{I}-\mathcal{T})^{-1} \left(\mathrm{e}^{-i\pi/6}\mathcal{T}^{[\hat{\mathrm{c}}(x)]} + \mathrm{e}^{i\pi/6}\mathcal{T}^{[\hat{\mathrm{a}}(x)]} \right) |\mathbf{1}\rangle \right\} , \tag{4.11}$$

for all $z = \mathrm{e}^{i2\pi\ell} \notin \Lambda_{\mathcal{T}}$. For mixing processes, this reduces to:

$$\mathsf{I}_{\mathrm{D}}(\ell) = -6\sqrt{3}\ \Re\left\{ \langle \boldsymbol{\pi}|\, \mathcal{T}^{[x]}\, (z\mathbb{I}-\mathcal{T})^{-1} \left(\mathrm{e}^{-i\pi/6}\mathcal{T}^{[\hat{\mathrm{c}}(x)]} + \mathrm{e}^{i\pi/6}\mathcal{T}^{[\hat{\mathrm{a}}(x)]} \right) |\mathbf{1}\rangle \right\} , \tag{4.12}$$

for any $x \in \mathcal{A}_{\mathrm{P}}$. Note that there are no powers of the TM that need to be calculated in either of these cases. Rather, *the DP is a direct fingerprint of the noniterated TMs*. The simple elegance of Eq. (4.11) relating the DP and TMs suggests that there is a link of fundamental conceptual importance between them. The examples to follow draw out this connection.

The important role that $\mathcal{T}$'s eigenvalues $\Lambda_{\mathcal{T}}$ play in the DP should now be clear: they are the poles of the resolvent matrix $(\zeta\mathbb{I}-\mathcal{T})^{-1}$ with $\zeta \in \mathbb{C}$. Since the DP is a simple function of the resolvent evaluated along the unit circle, $\Lambda_{\mathcal{T}}$ plays a critical organizational role in the DP's structure. Any peaks in the DP are shadows of the poles of the resolvent filtered through the appropriate row and column vectors and cast out radially onto the unit circle. Peaks in the DP become more diffuse as the corresponding eigenvalues withdraw towards the origin of the complex plane. They approach δ-functions as the corresponding eigenvalues approach the unit circle. §5's examples demonstrate this graphically.

(b) Bragg Reflections

The eigenvalues $\Lambda_{\rho(\mathcal{T})} \subset \Lambda_{\mathcal{T}}$ along the unit circle are responsible for Bragg peaks, and we treat this case now. For finite-N, the eigenvalues along the unit circle give rise to Dirichlet kernels. As $N \to \infty$, the analysis becomes somewhat simpler since the Dirichlet kernel and Fejér kernel both tend to δ-functions.

As $N \to \infty$, the summation over n in Eq. (4.4) divided by the total number of MLs becomes:

$$\lim_{N\to\infty} \sum_{n=1}^{N} \frac{N-n}{N} z^{-n} \mathcal{T}^{n-1} = z^{-1} \sum_{\eta=0}^{\infty} (\mathcal{T}/z)^{\eta} . \tag{4.13}$$

At this point, it is pertinent to use the recently developed spectral decomposition of $\mathcal{T}^L$ [67]. With the allowance that $0^{L-m} = \delta_{L-m,0}$ for the case that $0 \in \Lambda_{\mathcal{T}}$, this is:

$$\mathcal{T}^L = \sum_{\lambda\in\Lambda_{\mathcal{T}}} \sum_{m=0}^{\nu_\lambda - 1} \lambda^{L-m} \binom{L}{m} \mathcal{T}_\lambda\, (\mathcal{T}-\lambda\mathbb{I})^m , \tag{4.14}$$

where (i) $\mathcal{T}_\lambda$ is the projection operator associated with the eigenvalue λ given by the elementwise residue of the resolvent $(z\mathbb{I}-\mathcal{T})^{-1}$ at $z \to \lambda$, (ii) the index ν_λ of the eigenvalue λ is the size of the largest Jordan block associated with λ, and (iii) $\binom{L}{m} = \frac{1}{m!}\prod_{n=1}^{m}(L-n+1)$ is the generalized binomial coefficient. In terms of elementwise counter-clockwise contour integration, we have:

$$\mathcal{T}_\lambda = \frac{1}{2\pi i} \oint_{C_\lambda} (z\mathbb{I}-\mathcal{T})^{-1}\, dz , \tag{4.15}$$

where C_λ is any contour in the complex plane enclosing the point $z_0 = \lambda$—which may or may not be a singularity depending on the particular element of the resolvent matrix—but encloses no other singularities. Usefully, the projection operators are a mutually orthogonal set such that for

$\zeta, \lambda \in \Lambda_{\mathcal{T}}$, we have:

$$\mathcal{T}_\zeta \mathcal{T}_\lambda = \delta_{\zeta,\lambda} \mathcal{T}_\lambda \, .$$

The Perron–Frobenius theorem guarantees that all eigenvalues of the stochastic TM $\mathcal{T}$ lie on or within the unit circle. Moreover—and very important to our discussion on Bragg reflections—the eigenvalues on the unit circle are guaranteed to have an index of one. The indices of all other eigenvalues must be less than or equal to one more than the difference between their algebraic a_λ and geometric g_λ multiplicities. Specifically:

$$\nu_\lambda - 1 \leq a_\lambda - g_\lambda \leq a_\lambda - 1$$

and

$$\nu_\lambda = 1 \text{ if } |\lambda| = 1 \, .$$

Taking advantage of the index-one nature of the eigenvalues on the unit circle, we can define:

$$\Xi \equiv \sum_{\zeta \in \Lambda_{\rho(\mathcal{T})}} \zeta \mathcal{T}_\zeta$$

and

$$F \equiv \mathcal{T} - \Xi \, .$$

Then, the summation on the right-hand side of Eq. (4.13) becomes:

$$\sum_{\eta=0}^{\infty} (\mathcal{T}/z)^\eta = \left[\sum_{\eta=0}^{\infty} (F/z)^\eta \right] + \left[\sum_{\eta=0}^{\infty} (\Xi/z)^\eta \right] \, . \tag{4.16}$$

In the above, only the summation involving Ξ is capable of contributing δ-functions. And so, expanding this summation, yields:

$$\sum_{\eta=0}^{\infty} (\Xi/z)^\eta = \sum_{\lambda \in \Lambda_{\rho(\mathcal{T})}} \mathcal{T}_\lambda \sum_{\eta=0}^{\infty} (\lambda/z)^\eta \tag{4.17}$$

$$= \sum_{\lambda \in \Lambda_{\rho(\mathcal{T})}} \mathcal{T}_\lambda \sum_{\eta=0}^{\infty} \mathrm{e}^{i2\pi(\ell_\lambda - \ell)\eta} \, , \tag{4.18}$$

where ℓ_λ is related to λ by $\lambda = \mathrm{e}^{i2\pi\ell_\lambda}$ over some appropriate length-one ℓ-interval.

Using properties of the discrete-time Fourier transform [68], we can finally pull the δ-functions out of Eq. (4.18). In particular:

$$\sum_{\eta=0}^{\infty} \mathrm{e}^{i2\pi(\ell_\lambda - \ell)\eta} = \frac{1}{1 - \mathrm{e}^{i2\pi(\ell_\lambda - \ell)}} + \sum_{k=-\infty}^{\infty} \tfrac{1}{2} \delta(\ell - \ell_\lambda + k) \, . \tag{4.19}$$

Identifying the context of Eq. (4.19) within Eq. (4.4) shows that the potential δ-function at ℓ_λ (and at its integer-offset values) has magnitude:[7]

$$\begin{aligned} \Delta_\lambda &\equiv \lim_{\epsilon \to 0} \int_{\ell_\lambda - \epsilon}^{\ell_\lambda + \epsilon} \mathsf{I}(\ell) \, d\ell \\ &= -\sqrt{3} \; \Re \left\{ \lambda^{-1} \left[\left\langle \mathcal{T}_\lambda^{\hat{\mathrm{c}}(\mathcal{A})} \right\rangle \mathrm{e}^{-i\pi/6} + \left\langle \mathcal{T}_\lambda^{\hat{\mathrm{a}}(\mathcal{A})} \right\rangle \mathrm{e}^{i\pi/6} \right] \right\} \end{aligned} \tag{4.20}$$

contributed via the summation of Eq. (4.4), where:

$$\left\langle \mathcal{T}_\lambda^{\hat{\xi}(\mathcal{A})} \right\rangle \equiv \sum_{x_0 \in \mathcal{A}_\mathrm{P}} \langle \boldsymbol{\pi} | \, \mathcal{T}^{[x_0]} \mathcal{T}_\lambda \mathcal{T}^{[\hat{\xi}(x_0)]} \, | \mathbf{1} \rangle \, . \tag{4.21}$$

[7] By magnitude, we mean the ℓ-integral over the δ-function. If integrating with respect to a related variable, then the magnitude of the δ-function changes accordingly. As a simple example, integrating over $\omega = 2\pi\ell$ changes the magnitude of the δ-function by a factor of 2π.

Finally, considering Eq. (4.20) together with the contribution of the persistent Fejér kernel, the discrete part of the DP is given by:

$$\mathrm{I}_{\mathrm{B}}(\ell) = \sum_{k=-\infty}^{\infty} \sum_{\lambda \in \Lambda_{\rho(\mathcal{T})}} \left(\delta_{\lambda,1} + \Delta_\lambda\right) \delta(\ell - \ell_\lambda + k) \,, \tag{4.22}$$

where $\delta_{\lambda,1}$ is a Kronecker delta and $\delta(\ell - \ell_\lambda + k)$ is a Dirac δ-function.

In particular, the presence of the Bragg reflection at integer ℓ (zero frequency) depends strongly on whether the stacking process is mixing. In any case, the magnitude of these δ-functions at integer ℓ is $1 + \Delta_1$. For an ergodic process $\mathcal{T}_1 = |\mathbf{1}\rangle \langle \boldsymbol{\pi}|$, so we have:

$$\left\langle \mathcal{T}_1^{\hat{\xi}(\mathcal{A})} \right\rangle = \sum_{x_0 \in \mathcal{A}_{\mathrm{P}}} \langle \boldsymbol{\pi}| \, \mathcal{T}^{[x_0]} \, |\mathbf{1}\rangle \, \langle \boldsymbol{\pi}| \, \mathcal{T}^{[\hat{\xi}(x_0)]} \, |\mathbf{1}\rangle \,. \tag{4.23}$$

For *mixing* ABC-machines, $\langle \boldsymbol{\pi}| \, \mathcal{T}^{[x]} \, |\mathbf{1}\rangle = \Pr(x) = 1/3$ for all $x \in \mathcal{A}_{\mathrm{P}}$, giving $\left\langle \mathcal{T}_1^{\xi(\mathcal{A})} \right\rangle = 1/3$. Hence:

$$\begin{aligned} \Delta_1 &= -\frac{\sqrt{3}}{3} \, \Re\left\{ \mathrm{e}^{-i\pi/6} + \mathrm{e}^{i\pi/6} \right\} \\ &= -\frac{2\sqrt{3}}{3} \cos(\pi/6) \\ &= -1 \,, \end{aligned} \tag{4.24}$$

and the integer-ℓ δ-functions are extinguished for all mixing processes.

For *nonmixing* processes, the probability of each ML is *not* necessarily the same, and the magnitude of the δ-function at integer-ℓ will reflect the heterogeneity of the single-symbol statistics.

(c) Full Spectral Treatment of the Diffuse Spectrum

From Eq. (4.11), it is clear that the diffuse part of the DP is directly related to the resolvent $(z\mathbb{I} - \mathcal{T})^{-1}$ of the state-to-state TM evaluated along the unit circle. According to Riechers & Crutchfield [67] the resolvent can be expressed in terms of the projection operators:

$$(z\mathbb{I} - \mathcal{T})^{-1} = \sum_{\lambda \in \Lambda_{\mathcal{T}}} \sum_{m=0}^{\nu_\lambda - 1} \tfrac{1}{(z-\lambda)^{m+1}} \mathcal{T}_\lambda (\mathcal{T} - \lambda \mathbb{I})^m \,. \tag{4.25}$$

Hence, Eq. (4.11) can be expressed as:

$$\mathrm{I}_{\mathrm{D}}(\ell) = -2\sqrt{3} \, \Re\left\{ \sum_{\lambda \in \Lambda_{\mathcal{T}}} \sum_{m=0}^{\nu_\lambda - 1} \frac{1}{(z-\lambda)^{m+1}} \left[\left\langle \mathcal{T}_{\lambda,m}^{\hat{\mathrm{c}}(\mathcal{A})} \right\rangle \mathrm{e}^{-i\pi/6} + \left\langle \mathcal{T}_{\lambda,m}^{\hat{\mathrm{a}}(\mathcal{A})} \right\rangle \mathrm{e}^{i\pi/6} \right] \right\} \,, \tag{4.26}$$

where $\left\langle \mathcal{T}_{\lambda,m}^{\hat{\xi}(\mathcal{A})} \right\rangle$ is a complex-valued scalar:[8]

$$\left\langle \mathcal{T}_{\lambda,m}^{\hat{\xi}(\mathcal{A})} \right\rangle \equiv \sum_{x_0 \in \mathcal{A}_{\mathrm{P}}} \langle \boldsymbol{\pi}| \, \mathcal{T}^{[x_0]} \mathcal{T}_\lambda \, (\mathcal{T} - \lambda \mathbb{I})^m \, \mathcal{T}^{[\hat{\xi}(x_0)]} \, |\mathbf{1}\rangle \,. \tag{4.27}$$

Moreover, if $\left\langle \mathcal{T}_{\lambda,m}^{\hat{\mathrm{c}}(\mathcal{A})} \right\rangle = \left\langle \mathcal{T}_{\lambda,m}^{\hat{\mathrm{a}}(\mathcal{A})} \right\rangle$ for all λ and all m, then Eq. (4.26) simplifies to:

$$\mathrm{I}_{\mathrm{D}}(\ell) = -6 \, \Re\left\{ \sum_{\lambda \in \Lambda_{\mathcal{T}}} \sum_{m=0}^{\nu_\lambda - 1} \frac{\left\langle \mathcal{T}_{\lambda,m}^{\hat{\mathrm{c}}(\mathcal{A})} \right\rangle}{(z-\lambda)^{m+1}} \right\} \,. \tag{4.28}$$

[8] $\left\langle \mathcal{T}_{\lambda,m}^{\hat{\xi}(\mathcal{A})} \right\rangle$ is constant with respect to the relative layer displacement n. However, $\left\{ \left\langle \mathcal{T}_{\lambda,m}^{\hat{\xi}(\mathcal{A})} \right\rangle \right\}$ can be a function of a process's parameters.

Table 1. The limiting material structures for the IID Process. Key: DF - deformation fault; Ran - completely random stacking.

$q=0$	$q\approx 0$	$q=\bar{q}=\frac{1}{2}$	$\bar{q}\approx 0$	$\bar{q}=0$
$3C^-$	$3C^-/DF$	Ran	$3C^+/DF$	$3C^+$

5. Examples

To illustrate the theory, we treat in some detail three examples for which we previously [60] estimated the CFs directly from the HMM. Throughout the examples, we find it particularly revealing to plot the DP and TM eigenvalues via, what we call, the *coronal spectrogram*. This takes advantage of the fact that the DP is periodic in ℓ with period one and that the TM's eigenvalues lie on or within the unit circle in the complex plane. Thus, a coronal spectrogram is any frequency-dependent graph emanating radially from the unit circle, while the unit circle and its interior are concurrently used for its portion of the complex plane to plot the poles of the resolvent of the underlying process's transition dynamic. (Here, the poles of the resolvent are simply the eigenvalues $\Lambda_{\mathcal{T}}$ of $\mathcal{T}$, since $\mathcal{T}$ is finite dimensional.)

Coronal spectrograms plot the DP as a function of the polar angle $\omega = 2\pi\ell$. The radial extent of the corona is normalized to have the same maximal value for each figure here. With our particular interest in the DP of CPSs, we plot all eigenvalues in $\Lambda_{\mathcal{T}}$ as (red, online) dots and also plot all eigenvalues in Λ_{T} as (black) $\times$s. Note that $\Lambda_{\mathsf{T}} \subset \Lambda_{\mathcal{T}}$. In all of our examples, it appears that only the eigenvalues introduced in generating the ABC-machine from the Hägg-machine (dots without $\times$s through them) are capable of producing DP peaks. For *nonmixing* processes this is not true, since the Hägg-machine and ABC-machine share the same topology and the same set of eigenvalues.

(a) 3C Polytypes and Random ML Stacking: IID Process

The independent and identically distributed Hägg process is the simplest ML stacking process in a CPS that one can consider. Although we work out this example largely as a pedagogical exercise, in limiting cases it can be thought of as random deformation faulting in face-center cubic (FCC) (aka 3C) crystals.

We define the *independent and identically distributed* (IID) stacking process as such: when transitioning between adjacent MLs, a ML will be cyclically related to the previous ML with probability $q \in [0, 1]$. Due to stacking constraints, the ML will otherwise be anticyclically related to its predecessor with probability $\bar{q} \equiv 1 - q$.[9] The Hägg-machine and ABC-machine for the IID Process are given in Fig. 1.

It is useful to consider limiting cases for q. When $q = 0.5$, the stacking is completely random, subject only to the stacking constraints preventing two adjacent MLs from having the same orientation. As $q \to 1$, adjacent MLs are almost always cyclically related, and the specimen can be thought of as a $3C^+$ crystal with randomly distributed deformation faults [19] with probability $\bar{q}$. As $q \to 0$, it is also a 3C crystal with randomly distributed deformation faults, except that the MLs are anticyclically related, which we denote as $3C^-$. This is summarized in Table 1.

The TMs in ABC-notation are:

$$\mathcal{T}^{[A]} = \begin{bmatrix} 0 & 0 & 0 \\ \bar{q} & 0 & 0 \\ q & 0 & 0 \end{bmatrix}, \quad \mathcal{T}^{[B]} = \begin{bmatrix} 0 & q & 0 \\ 0 & 0 & 0 \\ 0 & \bar{q} & 0 \end{bmatrix} \quad \text{and} \quad \mathcal{T}^{[C]} = \begin{bmatrix} 0 & 0 & \bar{q} \\ 0 & 0 & q \\ 0 & 0 & 0 \end{bmatrix}.$$

[9] Here and in the following examples, we define a bar over a variable to mean one minus that variable: $\bar{x} \equiv 1 - x$.

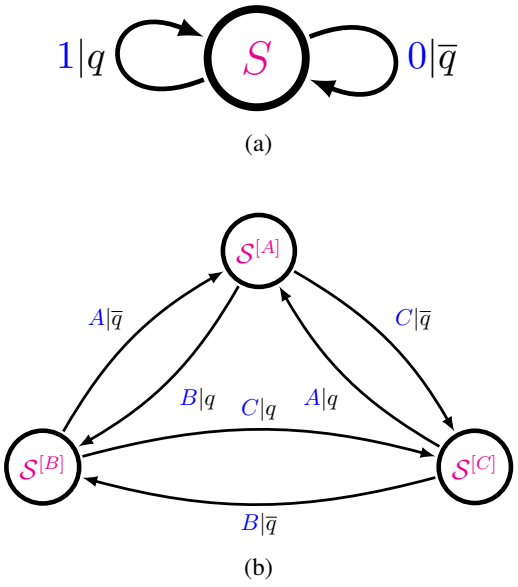

Figure 1. The (a) Hägg-machine and the (b) ABC-machine for the IID Process, $q \in [0,1]$. When $q = 1$, the IID process generates a string of 1s, which is physically the 3C$^+$ stacking structure. Conversely, for $q = 0$, the structure corresponds to the 3C$^-$ structure. For $q = 0.5$, the MLs are stacked as randomly as possible. Notice that the single state of the Hägg-machine has split into a three-state ABC-machine. This trebling of states is a generic feature of expanding mixing Hägg-machines into ABC-machines. It should be observed when written in the ABC-notation the process is actually a MM. Changing from one stacking notation to another can affect the order of the Markov model, and is discussed elsewhere [12]. (From Riechers *et al.* [60], used with permission.)

The internal state TM then is their sum:

$$\mathcal{T} = \begin{bmatrix} 0 & q & \overline{q} \\ \overline{q} & 0 & q \\ q & \overline{q} & 0 \end{bmatrix} .$$

The eigenvalues of the ABC TM are

$$\Lambda_{\mathcal{T}} = \{1,\, \Omega,\, \Omega^*\} ,$$

where:

$$\Omega \equiv -\frac{1}{2} + i\frac{\sqrt{3}}{2}(4q^2 - 4q + 1)^{1/2}$$

and Ω^* is its complex conjugate.

Furthermore, the stationary distribution over states of the ABC-machine can be found from $\langle \boldsymbol{\pi}| = \langle \boldsymbol{\pi}|\, \mathcal{T}$ to be:

$$\langle \boldsymbol{\pi}| = \begin{bmatrix} \frac{1}{3} & \frac{1}{3} & \frac{1}{3} \end{bmatrix} .$$

For $q \in (0,1)$, none of the eigenvalues in $\Lambda_{\mathcal{T}}$ besides unity lie on the unit circle of the complex plane, and so there is no possibility of Bragg reflections at non-integer ℓ. Moreover, since the process is mixing, the Bragg peak at integer ℓ is also absent. Thus we need only find the diffuse DP. To calculate the $\mathsf{I}_{\mathrm{D}}(\ell)$ as given in Eq. (4.11), we are only missing $(z\mathbb{I} - \mathcal{T})^{-1}$, which is given

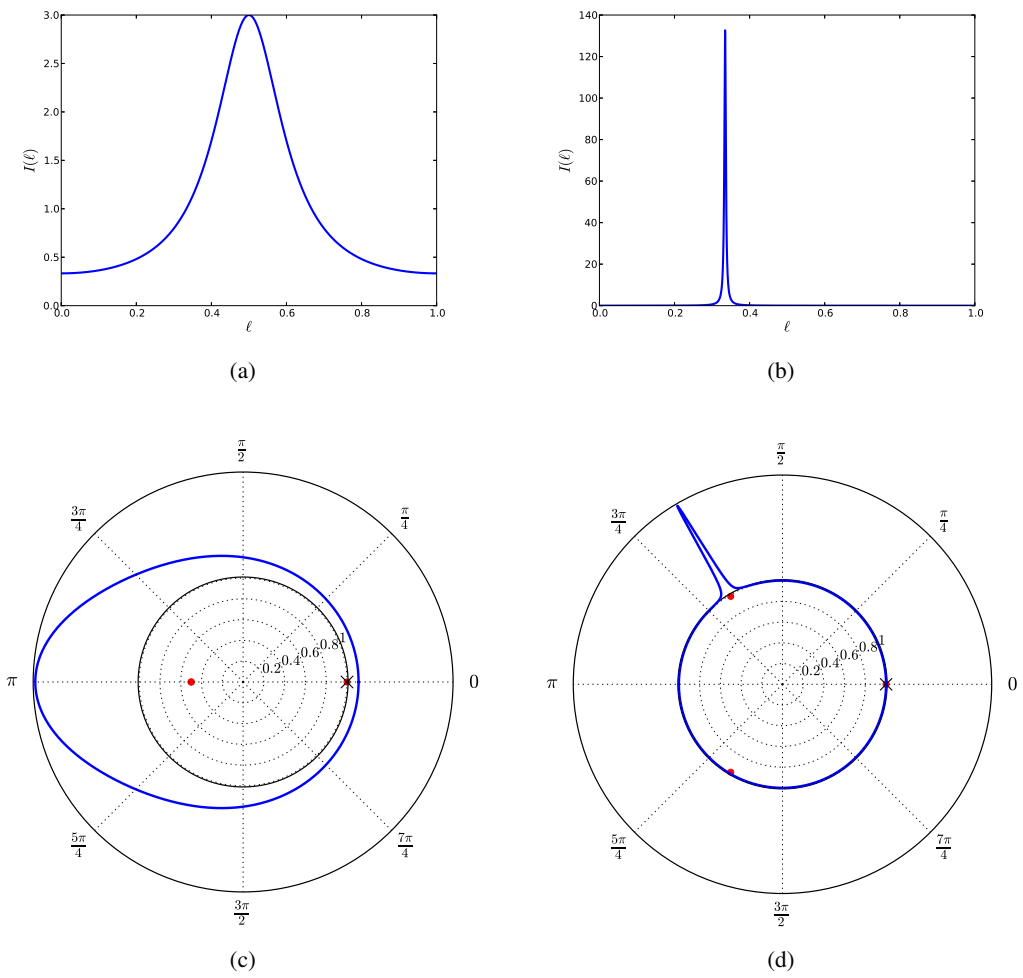

Figure 2. IID Process diffraction patterns for (a) $q = 0.5$ and (b) $q = 0.99$, as calculated from Eq. (5.2). Notice that as $q \to 1$, the DP approaches that of a 3C$^+$ crystal. For values of q close to but less than 1, the specimen is 3C$^+$ with randomly distributed deformation faults. (c) The coronal spectrogram corresponding to $q = 0.5$. The enhanced scattering at $\ell = 0.5$ in (a) is replaced with the bulge at $\omega = \pi$. There are three eigenvalues for the IID Process, one at $z = 1$ and a degenerate pair at $z = -0.5$. (d) The coronal spectrogram corresponding to $q = 0.99$. The Bragg-like peak at $\ell = 0.33$ in (b) is now represented as a Bragg-like peak at $\omega = 2\pi/3$. Notice how the degenerate eigenvalues in (c) have split and migrated away from the real axis. As they approach the boundary of the unit circle, their presence makes possible Bragg-like reflections in the DP. However, eigenvalues near the unit circle are a *necessary*, but *not sufficient* condition for Bragg-like reflections. This is seen in the eigenvalue in the third quadrant that is *not* accompanied by a Bragg-like reflection.

by:

$$(z\mathbb{I} - \mathcal{T})^{-1} = \frac{1}{(z-1)(z-\Omega)(z-\Omega^*)} \times \begin{bmatrix} z^2 - q\bar{q} & qz + \bar{q}^2 & \bar{q}z + q^2 \\ \bar{q}z + q^2 & z^2 - q\bar{q} & qz + \bar{q}^2 \\ qz + \bar{q}^2 & \bar{q}z + q^2 & z^2 - q\bar{q} \end{bmatrix} .$$

Then, with:

$$\langle \boldsymbol{\pi} | \, \mathcal{T}^{[A]} = \begin{bmatrix} \frac{1}{3} & 0 & 0 \end{bmatrix} ,$$

we can write

$$\langle \boldsymbol{\pi}| \, \mathcal{T}^{[A]} \, (z\mathbb{I} - \mathcal{T})^{-1} = \frac{1}{3} \frac{1}{(z-1)(z-\Omega)(z-\Omega^*)} \times \begin{bmatrix} z^2 - q\bar{q} & qz + \bar{q}^2 & \bar{q}z + q^2 \end{bmatrix},$$

where:

$$\mathcal{T}^{[\hat{c}(A)]} \, |\mathbf{1}\rangle = \mathcal{T}^{[B]} \, |\mathbf{1}\rangle = \begin{bmatrix} q \\ 0 \\ \bar{q} \end{bmatrix} \quad \text{and} \quad \mathcal{T}^{[\hat{a}(A)]} \, |\mathbf{1}\rangle = \mathcal{T}^{[C]} \, |\mathbf{1}\rangle = \begin{bmatrix} \bar{q} \\ q \\ 0 \end{bmatrix}.$$

From Eq. (4.12), the DP becomes:

$$\mathsf{I}_{\mathrm{D}}(\ell) = -\frac{6\sqrt{3}}{2} \, \Re \left\{ \frac{e^{i\pi/6} z \left(q^2 + \bar{q}z\right) + e^{-i\pi/6} z \left(\bar{q}^2 + qz\right)}{(z-1)(z-\Omega)(z-\Omega^*)} \right\} \tag{5.1}$$

$$= -2\sqrt{3} \, \Re \left\{ z \, \frac{e^{i\pi/6} \left(q^2 + \bar{q}z\right) + e^{-i\pi/6} \left(\bar{q}^2 + qz\right)}{(z-1)(z^2 + z + 1 - 3q\bar{q})} \right\}. \tag{5.2}$$

For the case of the most random possible stacking in CPSs, where $q = \bar{q} = \frac{1}{2}$, this simplifies to:

$$\mathsf{I}_{\mathrm{D}}(\ell) = \frac{3/4}{5/4 + \cos(2\pi\ell)}. \tag{5.3}$$

This result was obtained previously by more elementary means. The results are in agreement [20].

Figure 2 shows DPs and coronal spectrograms for $q = 0.5$ and $q = 0.99$. Figure 2(a) gives the DP for a maximally disordered stacking process. The spectrum is entirely diffuse with broadband enhancement near $\ell = 0.5$. In contrast, the DP for $q = 0.99$ in Fig. 2(b) shows a strong Bragg-like reflection at $\ell = 0.33$, which we recognize as just the $3\mathrm{C}^+$ stacking structure, with a small amount of (as it turns out in this case) deformation faulting. The other two panels in Fig. 2, (c) and (d), are coronal spectrograms giving DPs for these two cases as the radially emanating curve outside the unit circle, but now the three eigenvalues of the total TM are plotted interior to the unit circle. As always, there is a single eigenvalue at $z = 1$. In panel (c), the other two degenerate eigenvalues occur at $z = -0.5$, 'casting a shadow' on the unit circle in the form of enhanced power at $\omega = \pi$. In panel (d), these eigenvalues split and move away from the real axis closer to the unit circle. In doing so, one casts a more focused shadow in the form of a Bragg-like reflection at $\omega = 2\pi/3$. For $q = 1$, this eigenvalue finally comes to rest on the unit circle, and the Bragg-like reflection becomes a true Bragg peak, as explored shortly. Note that the other eigenvalue does not give rise to enhanced scattering. We find that having an eigenvalue near the unit circle is necessary to produce enhanced scattering, but the presence of such an eigenvalue does not necessarily guarantee Bragg-like reflections.

(i) Bragg Peaks from 3C

For the case of $q \in \{0, 1\}$, we recover perfect crystalline structure. Although the presence, placement, and magnitude of Bragg peaks are well known from other methods, we show the comprehensive consistency of our method via the example of $q = 1$ ($\bar{q} = 0$). In this case: $\Lambda_{\mathcal{T}} = \{1, \Omega, \Omega^*\}$ with $\Omega = -\frac{1}{2} + i\frac{\sqrt{3}}{2} = \mathrm{e}^{i2\pi/3}$, so that $\ell_{\Omega} = 1/3$ and $\ell_{\Omega^*} = 2/3$, and the two relevant projection operators reduce to:

$$\mathcal{T}_{\Omega} = \frac{1}{(\Omega-1)(\Omega-\Omega^*)} \begin{bmatrix} \Omega^2 & \Omega & 1 \\ 1 & \Omega^2 & \Omega \\ \Omega & 1 & \Omega^2 \end{bmatrix} \text{ and } \mathcal{T}_{\Omega^*} = \frac{1}{(\Omega^*-1)(\Omega^*-\Omega)} \begin{bmatrix} \Omega^{*2} & \Omega^* & 1 \\ 1 & \Omega^{*2} & \Omega^* \\ \Omega^* & 1 & \Omega^{*2} \end{bmatrix}.$$

From Eq. (4.21), we have:

$$\left\langle \mathcal{T}_{\Omega}^{\hat{c}(\mathcal{A})} \right\rangle = \frac{\Omega^2}{(\Omega-1)(\Omega-\Omega^*)}, \quad \left\langle \mathcal{T}_{\Omega}^{\hat{a}(\mathcal{A})} \right\rangle = \frac{\Omega}{(\Omega-1)(\Omega-\Omega^*)},$$

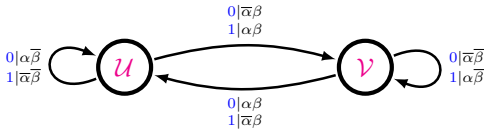

Figure 3. The Hägg-machine for the RGDF Process as proposed by Estevez *et al.* [69]. This two-state machine is a niMM and has two parameters, $\alpha \in [0,1]$ and $\beta \in [0,1]$, the probability of deformation and growth faults in CPSs, respectively. (From Riechers *et al.* [60], used with permission.)

Table 2. The limiting material structures for the RGDF Process. Key: GF - growth fault; DF - deformation fault; Ran - completely random stacking.

	$\beta = 0$	$\beta \approx 0$	$\beta = \bar{\beta} = 1/2$	$\bar{\beta} \approx 0$	$\bar{\beta} = 0$
$\alpha = 0$	3C	3C/GF	Ran	2H/GF	2H
$\alpha \approx 0$	3C/DF	3C/DF,GF	Ran	2H/DF,GF	2H/DF
$\alpha = \frac{1}{2}$	Ran	Ran	Ran	Ran	Ran

and

$$\left\langle T^{\hat{c}(\mathcal{A})}_{\Omega^*} \right\rangle = \frac{\Omega^{*2}}{(\Omega^* - 1)(\Omega^* - \Omega)} , \quad \left\langle T^{\hat{a}(\mathcal{A})}_{\Omega^*} \right\rangle = \frac{\Omega^*}{(\Omega^* - 1)(\Omega^* - \Omega)} ,$$

which from Eq. (4.20) yields:

$$\Delta_\Omega = 1 \quad \text{and} \quad \Delta_{\Omega^*} = 0 .$$

Then, using Eq. (4.22), the DP's discrete part becomes:

$$\mathrm{I}_\mathrm{B}(\ell) = \sum_{k=-\infty}^{\infty} \delta(\ell - \tfrac{1}{3} + k) ,$$

as it ought to be for $3\mathrm{C}^+$.

(b) Random Growth and Deformation Faults in Layered 3C and 2H CPSs: The RGDF Process

As a simple model of faulting in CPSs, combined random growth and deformation faults are often assumed if the faulting probabilities are believed to be small. However, until now there has not been an analytical expression available for the DP for all values of the faulting parameters, and we derive such an expression here.

The HMM for the *Random Growth and Deformation Faults* (RGDF) process was first proposed by Estevez-Rams *et al.* [69] and the Hägg-machine is shown in Fig. 3. The process has two parameters, $\alpha \in [0,1]$ and $\beta \in [0,1]$, that (at least for small values) are interpreted as the probability of deformation and growth faults, respectively. The stacking process, however, is described best on its own terms—in terms of the HMM, which captures the causal architecture of the stacking for all parameter values.

It is instructive to consider limiting values of α and β. For $\alpha = \beta = 0$, the stacking structure is simply 3C. The machine splits into two distinct machines: each machine has one state with a single self-state transition, corresponding to the $3\mathrm{C}^+$ stacking structure and the other to $3\mathrm{C}^-$ stacking structure. The 2H stacking structure occurs when $\alpha = \bar{\beta} = 0$. Typically growth faults are introduced as β strays from these limiting values, and deformation faults appear when α becomes small but nonvanishing. When $\alpha = 1/2$, the stacking becomes completely random, regardless of the value of β. This is summarized in Table 2.

The RGDF Hägg-machine's TMs are:

$$\mathsf{T}^{[0]} = \begin{bmatrix} \alpha\overline{\beta} & \overline{\alpha}\beta \\ \alpha\beta & \overline{\alpha}\overline{\beta} \end{bmatrix} \text{ and } \mathsf{T}^{[1]} = \begin{bmatrix} \overline{\alpha}\overline{\beta} & \alpha\beta \\ \overline{\alpha}\beta & \alpha\overline{\beta} \end{bmatrix}.$$

The Hägg-machine is nonmixing only for the parameter settings $\beta = 1$ and $\alpha \in \{0, 1\}$, giving rise to 2H crystal structure.

From the Hägg-machine, we obtain the corresponding TMs of the ABC-machine for $\alpha, \beta \in (0, 1)$ [60]:

$$\mathcal{T}^{[A]} = \begin{bmatrix} 0 & 0 & 0 & 0 & 0 & 0 \\ \alpha\overline{\beta} & 0 & 0 & \overline{\alpha}\beta & 0 & 0 \\ \overline{\alpha}\overline{\beta} & 0 & 0 & \alpha\beta & 0 & 0 \\ 0 & 0 & 0 & 0 & 0 & 0 \\ \alpha\beta & 0 & 0 & \overline{\alpha}\overline{\beta} & 0 & 0 \\ \overline{\alpha}\beta & 0 & 0 & \alpha\overline{\beta} & 0 & 0 \end{bmatrix}, \quad \mathcal{T}^{[B]} = \begin{bmatrix} 0 & \overline{\alpha}\overline{\beta} & 0 & 0 & \alpha\beta & 0 \\ 0 & 0 & 0 & 0 & 0 & 0 \\ 0 & \alpha\overline{\beta} & 0 & 0 & \overline{\alpha}\beta & 0 \\ 0 & \overline{\alpha}\beta & 0 & 0 & \alpha\overline{\beta} & 0 \\ 0 & 0 & 0 & 0 & 0 & 0 \\ 0 & \alpha\beta & 0 & 0 & \overline{\alpha}\overline{\beta} & 0 \end{bmatrix}$$

and

$$\mathcal{T}^{[C]} = \begin{bmatrix} 0 & 0 & \alpha\overline{\beta} & 0 & 0 & \overline{\alpha}\beta \\ 0 & 0 & \overline{\alpha}\overline{\beta} & 0 & 0 & \alpha\beta \\ 0 & 0 & 0 & 0 & 0 & 0 \\ 0 & 0 & \alpha\beta & 0 & 0 & \overline{\alpha}\overline{\beta} \\ 0 & 0 & \overline{\alpha}\beta & 0 & 0 & \alpha\overline{\beta} \\ 0 & 0 & 0 & 0 & 0 & 0 \end{bmatrix},$$

and the orientation-agnostic state-to-state TM:

$$\mathcal{T} = \mathcal{T}^{[A]} + \mathcal{T}^{[B]} + \mathcal{T}^{[C]}.$$

Explicitly, we have:

$$\mathcal{T} = \begin{bmatrix} 0 & \overline{\alpha}\overline{\beta} & \alpha\overline{\beta} & 0 & \alpha\beta & \overline{\alpha}\beta \\ \alpha\overline{\beta} & 0 & \overline{\alpha}\overline{\beta} & \overline{\alpha}\beta & 0 & \alpha\beta \\ \overline{\alpha}\overline{\beta} & \alpha\overline{\beta} & 0 & \alpha\beta & \overline{\alpha}\beta & 0 \\ 0 & \overline{\alpha}\beta & \alpha\beta & 0 & \alpha\overline{\beta} & \overline{\alpha}\overline{\beta} \\ \alpha\beta & 0 & \overline{\alpha}\beta & \overline{\alpha}\overline{\beta} & 0 & \alpha\overline{\beta} \\ \overline{\alpha}\beta & \alpha\beta & 0 & \alpha\overline{\beta} & \overline{\alpha}\overline{\beta} & 0 \end{bmatrix}.$$

$\mathcal{T}$'s eigenvalues satisfy $\det(\mathcal{T} - \lambda\mathbb{I}) = 0$, from which we obtain the eigenvalues [60]:

$$\Lambda_{\mathcal{T}} = \left\{1,\ 1 - 2\beta,\ -\tfrac{1}{2}(1 - \beta) \pm \tfrac{1}{2}\sqrt{\sigma}\right\}, \tag{5.4}$$

with

$$\sigma \equiv 4\beta^2 - 3\overline{\beta}^2 + 12\alpha\overline{\alpha}(\overline{\beta} - \beta) \tag{5.5}$$

$$= -3 + 12\alpha + 6\beta - 12\alpha^2 + \beta^2 - 24\alpha\beta + 24\alpha^2\beta. \tag{5.6}$$

Except for measure-zero submanifolds along which the eigenvalues become extra degenerate, throughout the parameter range the eigenvalues' algebraic multiplicities are: $a_1 = 1$, $a_{1-2\beta} = 1$, $a_{-\frac{1}{2}(1-\beta+\sqrt{\sigma})} = 2$, and $a_{-\frac{1}{2}(1-\beta-\sqrt{\sigma})} = 2$. Moreover, the *index* of all eigenvalues is 1 except along $\sigma = 0$. Hence, due to their qualitative difference, we treat the cases of $\sigma = 0$ and $\sigma \neq 0$ separately.

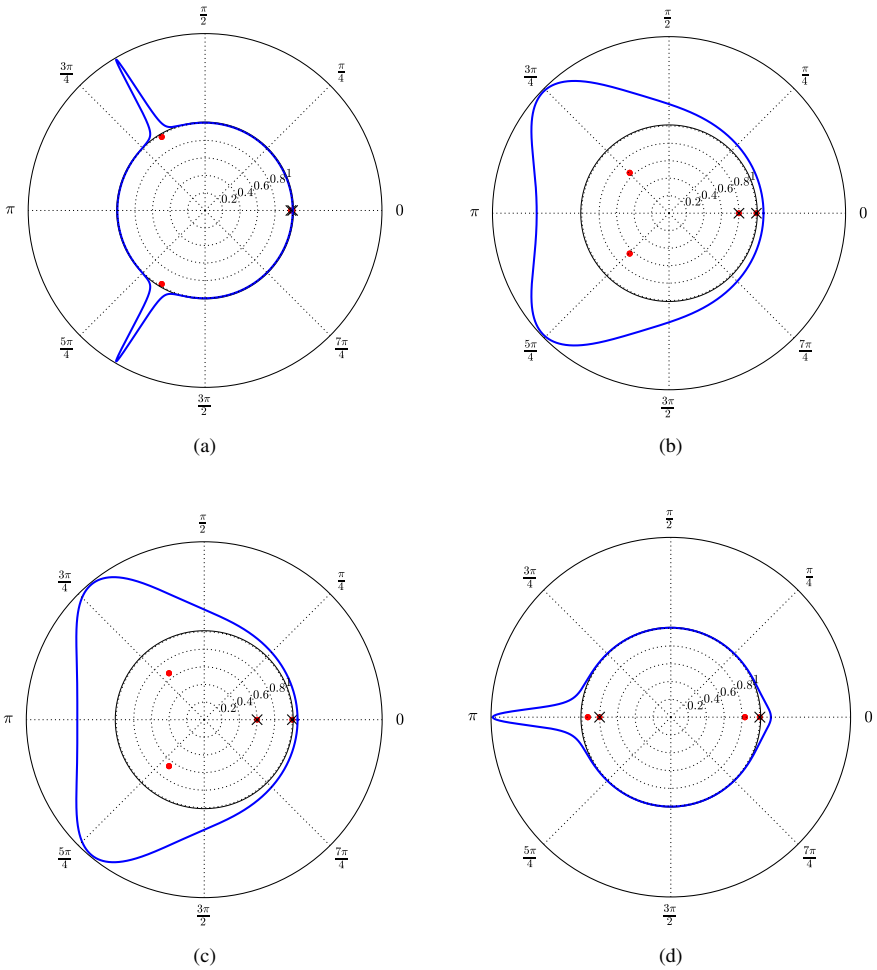

Figure 4. Coronal spectrograms showing the DP and eigenvalues for the RGDF Process: (a) $\alpha = 0.01$, $\beta = 0.01$; (b) $\alpha = 0.2$, $\beta = 0.1$; (c) $\alpha = 0.1$, $\beta = 0.2$; and (d) $\alpha = 0.01$, $\beta = 0.9$. Note how the eigenvalues organize the DP: as the eigenvalues approach the unit circle, the DP becomes enhanced. Also, note that nowhere is there enhanced scattering without an underlying eigenvalue of the TM driving it.

(i) $\sigma = 0$:

Riechers *et al.* [60] found that:

$$\left\langle \mathcal{T}_1^{\hat{\mathrm{c}}(\mathcal{A})} \right\rangle = \left\langle \mathcal{T}_1^{\hat{\mathrm{a}}(\mathcal{A})} \right\rangle = \tfrac{1}{3} \,, \quad \left\langle \mathcal{T}_{1-2\beta}^{\hat{\mathrm{c}}(\mathcal{A})} \right\rangle = \left\langle \mathcal{T}_{1-2\beta}^{\hat{\mathrm{a}}(\mathcal{A})} \right\rangle = 0 \,, \quad \left\langle \mathcal{T}_{-\overline{\beta}/2}^{\hat{\mathrm{c}}(\mathcal{A})} \right\rangle = \left\langle \mathcal{T}_{-\overline{\beta}/2}^{\hat{\mathrm{a}}(\mathcal{A})} \right\rangle = \tfrac{1}{6} \,,$$

and

$$\left\langle \mathcal{T}_{-\overline{\beta}/2,1}^{\hat{\mathrm{c}}(\mathcal{A})} \right\rangle = \left\langle \mathcal{T}_{-\overline{\beta}/2,1}^{\hat{\mathrm{a}}(\mathcal{A})} \right\rangle = -\tfrac{1}{12}\beta\overline{\beta} \,,$$

for the case of $\sigma = 0$. According to Eq. (4.28), the DP for $\sigma = 0$ is thus:

$$\begin{aligned}
\mathsf{I}_{\mathrm{D}}(\ell) &= -6\ \Re\left\{\sum_{\lambda\in\Lambda_{\mathcal{T}}}\sum_{m=0}^{\nu_\lambda-1}\frac{\left\langle \mathcal{T}^{\hat{\mathrm{c}}(\mathcal{A})}_{\lambda,m}\right\rangle}{(z-\lambda)^{m+1}}\right\}\\
&= -6\ \Re\left\{\frac{\left\langle \mathcal{T}^{\hat{\mathrm{c}}(\mathcal{A})}_{1}\right\rangle}{z-1}+\frac{\left\langle \mathcal{T}^{\hat{\mathrm{c}}(\mathcal{A})}_{-\bar{\beta}/2}\right\rangle}{z+\bar{\beta}/2}+\frac{\left\langle \mathcal{T}^{\hat{\mathrm{c}}(\mathcal{A})}_{-\bar{\beta}/2,1}\right\rangle}{(z+\bar{\beta}/2)^2}\right\}\\
&= \Re\left\{-\frac{2}{z-1}-\frac{1}{z+\bar{\beta}/2}+\frac{\beta\bar{\beta}/2}{(z+\bar{\beta}/2)^2}\right\}\\
&= 1-\ \Re\left\{\frac{z+\bar{\beta}^2/2}{(z+\bar{\beta}/2)^2}\right\}\ .
\end{aligned}\tag{5.7}$$

(ii) $\sigma \neq 0$:

Riechers *et al.* [60] also found that:

$$\left\langle \mathcal{T}^{\hat{\mathrm{c}}(\mathcal{A})}_{1}\right\rangle = \left\langle \mathcal{T}^{\hat{\mathrm{a}}(\mathcal{A})}_{1}\right\rangle = \tfrac{1}{3},\quad \left\langle \mathcal{T}^{\hat{\mathrm{c}}(\mathcal{A})}_{1-2\beta}\right\rangle = \left\langle \mathcal{T}^{\hat{\mathrm{a}}(\mathcal{A})}_{1-2\beta}\right\rangle = 0\,,$$

$$\left\langle T^{\hat{\mathrm{c}}(\mathcal{A})}_{\frac{-\bar{\beta}+\sqrt{\sigma}}{2}}\right\rangle = \left\langle T^{\hat{\mathrm{a}}(\mathcal{A})}_{\frac{-\bar{\beta}+\sqrt{\sigma}}{2}}\right\rangle = -\tfrac{1}{12}\left(1-\frac{\beta}{\sqrt{\sigma}}\right)\left(\sqrt{\sigma}-\overline{\beta}\right)\ ,$$

and

$$\left\langle T^{\hat{\mathrm{c}}(\mathcal{A})}_{\frac{-\bar{\beta}-\sqrt{\sigma}}{2}}\right\rangle = \left\langle T^{\hat{\mathrm{a}}(\mathcal{A})}_{\frac{-\bar{\beta}-\sqrt{\sigma}}{2}}\right\rangle = \tfrac{1}{12}\left(1+\frac{\beta}{\sqrt{\sigma}}\right)\left(\sqrt{\sigma}+\overline{\beta}\right)\ ,$$

for $\sigma \neq 0$. According to Eq. (4.28), the DP for $\sigma \neq 0$ is:

$$\begin{aligned}
\mathsf{I}_{\mathrm{D}}(\ell) &= -6\ \Re\left\{\sum_{\lambda\in\Lambda_{\mathcal{T}}}\frac{\left\langle \mathcal{T}^{\hat{\mathrm{c}}(\mathcal{A})}_{\lambda}\right\rangle}{z-\lambda}\right\}\\
&= -6\ \Re\left\{\frac{\left\langle \mathcal{T}^{\hat{\mathrm{c}}(\mathcal{A})}_{1}\right\rangle}{z-1}+\frac{\left\langle \mathcal{T}^{\hat{\mathrm{c}}(\mathcal{A})}_{\frac{-\bar{\beta}+\sqrt{\sigma}}{2}}\right\rangle}{z-\frac{\sqrt{\sigma}-\bar{\beta}}{2}}+\frac{\left\langle \mathcal{T}^{\hat{\mathrm{c}}(\mathcal{A})}_{\frac{-\bar{\beta}-\sqrt{\sigma}}{2}}\right\rangle}{z+\frac{\sqrt{\sigma}+\bar{\beta}}{2}}\right\}\\
&= 1+\tfrac{1}{2}\ \Re\left\{\frac{1-\beta/\sqrt{\sigma}}{\frac{z}{\sqrt{\sigma}-\bar{\beta}}-\frac{1}{2}}-\frac{1+\beta/\sqrt{\sigma}}{\frac{z}{\sqrt{\sigma}+\beta}+\frac{1}{2}}\right\}\ .
\end{aligned}\tag{5.8}$$

Figure 4 gives several coronal spectrograms for various values of the parameters α and β. It is instructive to examine the influence of the TM's eigenvalues on the placement and intensity of the Bragg-like reflections. In panel (a) there are two strong reflections, one each at $\omega = 2\pi/3$ and $4\pi/3$, signaling a twinned 3C structure, when the faulting parameters are set to $\alpha = \beta = 0.01$. Each is accompanied by an eigenvalue close to the surface of the unit circle. As the disorder is increased, see panels (b) and (c), TM eigenvalues retreat toward the center of the unit circle and the two strong reflections become diffuse. However, in the final panel (d), the faulting parameters ($\alpha = 0.01$, $\beta = 0.9$) are set such that the material has apparently undergone a phase transition from prominently 3C stacking structure to prominently 2H stacking structure. Indeed, the eigenvalues have coalesced through the critical point of $\sigma = 0$ (as σ changes from negative to positive) and emerge on the other side of the phase transition mutually scattered along the real axis and approaching the edge of the unit circle, giving rise to the 2H-like protrusions in the DP. This demonstrates again how the eigenvalues orchestrate the placement and intensity of the Bragg-like peaks.

Table 3. Limiting material structures for the SFSF Process. Key: SF - Shockley–Frank fault; NGF - nonrandom growth fault.

$\gamma = 0$	$\gamma \approx 0$	$\bar{\gamma} \approx 0$	$\bar{\gamma} = 0$
6H	6H/SF	3C/NGF	3C

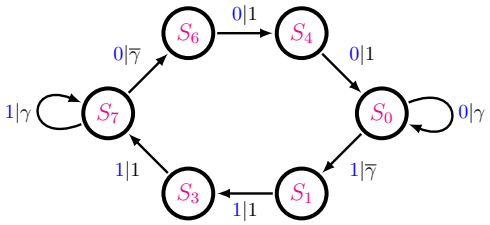

Figure 5. The Hägg-machine for the SFSF Process expressed as a 3rd-order MM. There is one faulting parameter $\gamma \in [0, 1]$ and three SSCs or, equivalently, three CSCs, as this machine is also an ϵ-machine. The three SSCs are $[S_7]$, $[S_0]$ and $[S_7S_6S_4S_0S_1S_3]$. The latter we recognize as the 6H structure if $\gamma = 0$. For large values of γ—*i.e.*, as $\gamma \to 1$—this process approaches a twinned 3C structure, although the faulting is *not* random. The causal-state architecture prevents the occurrence of domains of size-three or less. (From Riechers *et al.* [60] Used with permission.)

(c) Shockley–Frank Stacking Faults in 6H-SiC: The SFSF Process

SiC has been the intense focus of both experimental and theoretical investigations for some time due to its promise as a material suitable for next-generation electronic devices. However, it is known that SiC can have many different stacking configurations—some ordered and some disordered [4]—and these different stacking configurations can profoundly affect material properties. Despite considerable effort to grow commercial SiC wafers that are purely crystalline—*i.e.*, that have no stacking defects—reliable techniques have not yet been developed. It is therefore important to better understand and characterize the nature of the defects in order to better control them.

Recently, Sun *et al.* [70] reported experiments on 6H-SiC that used a combination of low temperature photoluminescence and high resolution transmission electron microscopy (HRTEM). One of the more common crystalline forms of SiC, the 6H stacking structure is simply the sequence ...ABCACBA ..., or in terms of the Hägg-notation, ...111000 .... The most common stacking fault in 6H-SiC identified by HRTEM can be explained as the result of one extrinsic Frank stacking fault coupled with one Shockley stacking fault [9]. Physically, the resultant stacking structure corresponds to the insertion of an additional SiC ML so that one has instead ...110000$\underline{0}$111000 ..., where the underlined spin is the inserted ML.

Inspired by these findings, we suggest a simple HMM for the *Shockley–Frank stacking fault* (SFSF) process that replicates this structure, and this is shown in Fig. 5. Our motivation here is largely pedagogical, and certainly more detailed experiments are required to confidently propose a structure, but this HMM reproduces at least qualitatively the observed structure. The model has a single parameter $\gamma \in [0, 1]$. As before, it is instructive to consider limiting cases of γ. For $\gamma = 0$, we have the pure 6H structure and, for small γ, Shockley–Frank defects are introduced into this stacking structure. As $\gamma \to 1$, the structure transitions into a twinned 3C crystal. However, unlike the previous example, this twinning is not random. Instead, the architecture of the machine requires that at least three 0s or 1s must be seen before there is a possibility of reversing the chirality, *i.e.*, before there is twinning. These limiting cases are summarized in Table 3.

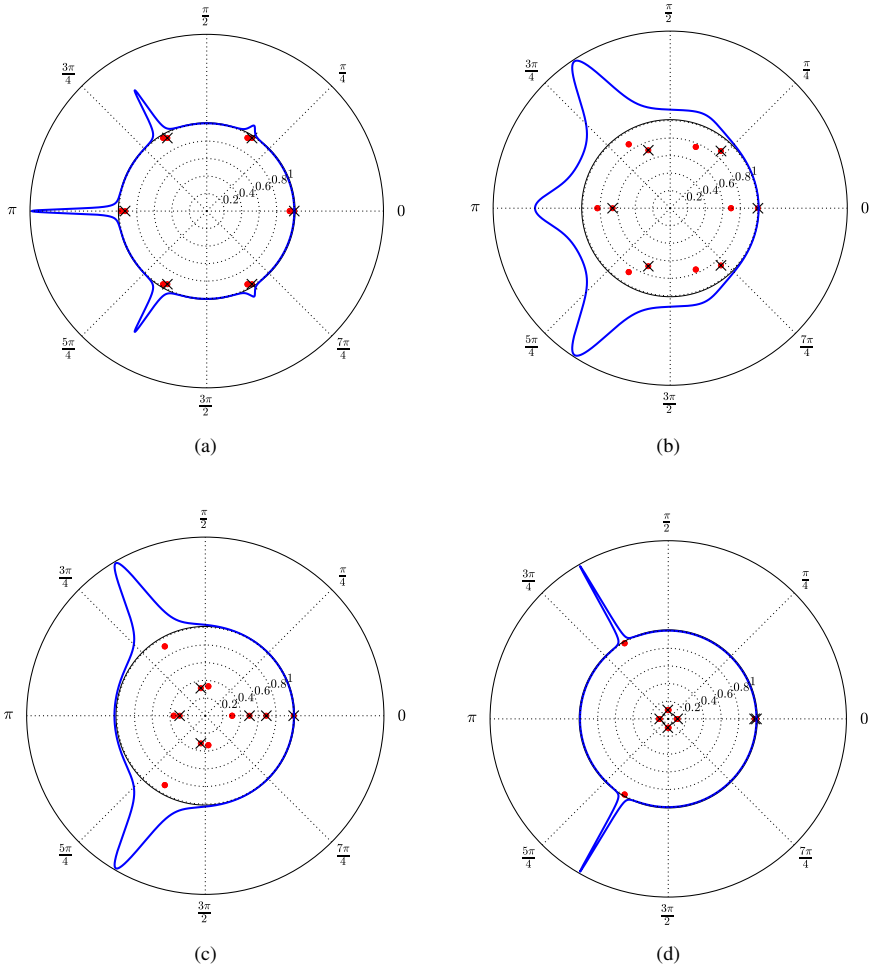

Figure 6. Coronal spectrograms showing the evolution of the DP and its eigenvalues for the SFSF Process. (a) $\gamma = 0.1$, (b) $\gamma = 0.5$, (c) $\gamma = 0.9$, and (d) $\gamma = 0.99$. In (a) the faulting is weak and the DP has the six degraded Bragg-like reflections characteristic of the 6H stacking structure. In (b), the faulting is more severe, with the concomitant erosion of the Bragg-like reflections, especially for $\omega = \pi$. In panel (c) the 6H character has been eliminated, and the Bragg-like peaks at $\omega = 2\pi/3$ and $4\pi/3$ are now associated with a twinned 3C stacking structure. In panel (d), the Bragg-like reflections sharpen as the probability of short 3C sequences stacking sequences decreases.

For $\gamma \in (0, 1)$ the Hägg-machine is mixing and we proceed with this case. By inspection, we write down the two 6-by-6 TMs of the Hägg-machine as:

$$\mathsf{T}^{[0]} = \begin{bmatrix} \gamma & 0 & 0 & 0 & 0 & 0 \\ 0 & 0 & 0 & 0 & 0 & 0 \\ 0 & 0 & 0 & 0 & 0 & 0 \\ 0 & 0 & 0 & 0 & \overline{\gamma} & 0 \\ 0 & 0 & 0 & 0 & 0 & 1 \\ 1 & 0 & 0 & 0 & 0 & 0 \end{bmatrix} \quad \text{and} \quad \mathsf{T}^{[1]} = \begin{bmatrix} 0 & \overline{\gamma} & 0 & 0 & 0 & 0 \\ 0 & 0 & 1 & 0 & 0 & 0 \\ 0 & 0 & 0 & 1 & 0 & 0 \\ 0 & 0 & 0 & \gamma & 0 & 0 \\ 0 & 0 & 0 & 0 & 0 & 0 \\ 0 & 0 & 0 & 0 & 0 & 0 \end{bmatrix},$$

where the states are ordered S_0, S_1, S_3, S_7, S_6, and S_4. The internal state TM is their sum:

$$\mathsf{T} = \begin{bmatrix} \gamma & \overline{\gamma} & 0 & 0 & 0 & 0 \\ 0 & 0 & 1 & 0 & 0 & 0 \\ 0 & 0 & 0 & 1 & 0 & 0 \\ 0 & 0 & 0 & \gamma & \overline{\gamma} & 0 \\ 0 & 0 & 0 & 0 & 0 & 1 \\ 1 & 0 & 0 & 0 & 0 & 0 \end{bmatrix}.$$

Since the six-state Hägg-machine generates an $(3 \times 6 =)$ eighteen-state ABC-machine, we do not explicitly write out its TMs. Nevertheless, it is straightforward to expand the Hägg-machine to the ABC-machine via the rote expansion method [60]. It is also straightforward to apply Eq. (4.12) to obtain the DP as a function of the faulting parameter γ. To use Eq. (4.12), note that the stationary distribution over the ABC-machine can be obtained from Eq. (A 1) with:

$$\langle \boldsymbol{\pi}_{\mathrm{H}}| = \tfrac{1}{6-4\overline{\gamma}} \begin{bmatrix} 1 & \overline{\gamma} & \overline{\gamma} & 1 & \overline{\gamma} & \overline{\gamma} \end{bmatrix}$$

as the stationary distribution over the Hägg-machine.

The eigenvalues of the Hägg TM can be obtained as the solutions of $\det(\mathsf{T} - \lambda\mathbb{I}) = (\lambda - \gamma)^2\lambda^4 - \overline{\gamma}^2 = 0$. These include 1, $-\frac{1}{2}\overline{\gamma} \pm \sqrt{\gamma^2 + 2\gamma - 3}$, and three other eigenvalues involving cube roots.

The eigenvalues of the ABC TM are obtained similarly as the solutions of $\det(\mathcal{T} - \lambda\mathbb{I}) = 0$. Note that $\Lambda_{\mathcal{T}}$ inherits Λ_{T} as the backbone for its more complex structure, just as $\Lambda_{\mathsf{T}} \subseteq \Lambda_{\mathcal{T}}$ for all of our previous examples. The eigenvalues in $\Lambda_{\mathcal{T}}$ are, of course, those most directly responsible for the structure of the CFs. Since the ABC-machine has eighteen states, there are eighteen eigenvalues contributing to the behavior of the DP; although several eigenvalues are degenerate. Hence, the SFSF Process is capable of a richer DP than the previous two examples.

The coronal spectrograms for the SFSF Process are shown for several example values of γ in Fig. 6. Over the range of γ values the stacking structure changes from a nearly perfect 6H crystal through a disordered phase finally becoming a twinned 3C structure. Most notable in Fig. 6 is how the eigenvalues of the total TM dictate the placement of the Bragg-like reflections. Phrased alternatively, the Bragg-like reflections appear to literally track the movement of the eigenvalues as they evolve during transformation.

6. Conclusions

We showed how the DP of layered CPSs, as described by an arbitrary HMM stacking process, is calculated either analytically or to a high degree of numerical certainty directly without restriction to finite-Markov-order and without needing finite samples of the stacking sequence. Our expressions for the DP are similar to those previously obtained by Treacy *et al.* [33], but since our our starting point is an arbitrary HMM, ours are guaranteed to be valid for both finite- and infinite-order Markov models. Along the way, we uncovered a remarkably simple relationship between the DP and the HMM. The former is given by straightforward, standard matrix manipulations of the latter. Critically, in the case of an infinite number of MLs, this relationship does not involve powers of the TM.

The connection yields important insights. (i) The number of Bragg and Bragg-like reflections in the DP is limited by the size of the TMs that define the HMM. Thus, knowing only the number of machine states reveals the maximum possible number of Bragg and Bragg-like reflections. (ii) As a corollary, given a DP, the number of Bragg and Bragg-like reflections puts a minimum on the number of HMM states. For the problem of inferring the HMM from experimental DPs, this gives powerful clues about the HMM (and so internal mechanism) architecture. (iii) The eigenvalues *within* the unit circle organize the diffuse Bragg-like reflections. Only TM eigenvalues *on* the unit circle correspond to those ℓ-values that potentially can result in true Bragg peaks. (iv) The expansion of the Hägg-machine into the ABC-machine, necessary for the appropriate matrix

manipulations, showed that there are two kinds of machines and, hence, two kinds of stacking process important in CPSs: mixing and nonmixing processes. In addition to the calculational shortcuts given by the former, mixing machines ensure that there are no true Bragg reflections at integer-ℓ. (v) Conversely, the presence of Bragg peaks at integer-ℓ is an unmistakable sign that a stacking process is nonmixing. Again, this puts important constraints on the HMM state architecture, useful for the problem of inverting the DP to find the HMM. (vi) For mixing processes, the ML probabilities must all be one-third, *i.e.*, $\Pr(A) = \Pr(B) = \Pr(C) = 1/3$.

New in the theory is the introduction of coronal spectrograms, a convenient way to visualize the interplay between a frequency-domain functional of a process and the eigenvalues of the process's TMs. In our case, the frequency-domain functional was the DP: the power spectrum of the sequence of ML structure factors. In each of the examples, the movement of the eigenvalues (as the HMM parameters change) were echoed by movement of their 'shadow'—the Bragg-like peaks in the power spectrum. While this technique was explored in the context of DPs from layered materials, this visualization tool is by no means confined to DPs or layered materials. We suspect that in other areas where power spectra and HMMs are studied, this technique will become a useful analysis tool.

There are several important research directions to follow in further refining and extending the theory and developing applications. (i) While specialized to CPSs here, the basic techniques extend to other stacking geometries and other materials, including the gamut of technologically cutting-edge heterostructures of stacked 2D materials. (ii) With the ability to analytically calculate DPs and CFs [60] from arbitrary HMMs, the number of physical and information- and computation-theoretic quantities amenable to such a treatment continues to expand. Statistical complexity, the Shannon entropy rate, and memory length have long been calculable from the ϵ-machine [29,43,50,51], but recently the excess entropy, transient information, and synchronization time have also been shown to be exactly calculable from the ϵ-machine [67,71]. This portends well that additional quantities, especially those of physical import such as band structure in chaotic crystals, may also be treatable with exact methods. (iii) Improved calculational techniques raise the possibility of improved inference methods, so that more kinds of stacking process may be discovered from DPs. An important research direction then is to incorporate these improved methods into more flexible, more sensitive inference algorithms.

Finally, the spectral methods pursued here increase the tools available to chaotic crystallography for the discovery, description, and categorization of both ordered and disordered (chaotic) crystals. With these tools in hand, we will more readily identify key features of the hidden structures responsible for novel physical properties of materials.

Acknowledgments

JPC thanks the Santa Fe Institute for hospitality during visits. JPC is an External Faculty member there. This material is based upon work supported by, or in part by, the U. S. Army Research Laboratory and the U. S. Army Research Office under contract number W911NF-13-1-0390.

A. Hägg-to-ABC Machine Translation

If M_H is the number of states in the Hägg-machine and M is the number of states in the ABC-machine, then $M = 3\mathsf{M}_\mathrm{H}$ for mixing Hägg-machines. Let the i^{th} state of the Hägg-machine split into the $(3i-2)^{\mathrm{th}}$ through the $(3i)^{\mathrm{th}}$ states of the corresponding ABC-machine. Then, each labeled-edge transition from the i^{th} to the j^{th} states of the Hägg-machine maps into a 3-by-3 submatrix for each of the three labeled TMs of the ABC-machine as:

$$\left\{\mathsf{T}^{[0]}_{ij}\right\} \xRightarrow{\text{Hägg to } ABC} \left\{\mathcal{T}^{[A]}_{3i-1,3j-2},\ \mathcal{T}^{[B]}_{3i,3j-1},\ \mathcal{T}^{[C]}_{3i-2,3j}\right\}$$

and

$$\left\{\mathsf{T}^{[1]}_{ij}\right\} \xRightarrow{\text{Hägg to } ABC} \left\{\mathcal{T}^{[A]}_{3i,3j-2},\ \mathcal{T}^{[B]}_{3i-2,3j-1},\ \mathcal{T}^{[C]}_{3i-1,3j}\right\}.$$

For nonmixing Hägg-machines, the above algorithm creates three disconnected ABC-machines, of which only one need be retained.

Furthermore, for mixing Hägg-machines, the probability from the stationary distribution over their states maps to a triplet of probabilities for the stationary distribution over the ABC-machine states:

$$\left\{p_i^{\mathrm{H}}\right\} \xrightarrow{\text{Hägg to } ABC} \{3p_{3i-2},\ 3p_{3i-1},\ 3p_{3i}\}\ . \tag{A 1}$$

A thorough exposition of these procedures is given by Riechers *et al.* [60].

References

1. A. K. Geim and I. V. Grigorieva, "Van der Waals heterostructures," *Nature*, vol. 499, pp. 419–425, 2013.
2. J. Liu, M. Kargarian, M. Kareev, B. Gray, P. J. Ryan, A. Cruz, N. Tahir, Y.-D. Chuang, J. Guo, J. M. Rondinelli, J. W. Freeland, G. A. Fiete, and J. Chakhalian, "Heterointerface engineered electronic and magnetic phases of $NdNiO_3$ thin films," *Nat. Comm.*, vol. 4, p. 2714, 2013.
3. Y. Kuwahara, "Comparison of the surface structure of the tetrahedral sheets of muscovite and phlogopite by AFM," *Physics and Chemistry of Minerals*, vol. 28, no. 1, pp. 1–8, 2001.
4. M. T. Sebastian and P. Krishna, *Random, Non-Random and Periodic Faulting in Crystals*. The Netherlands: Gordon and Breach, 1994.
5. F. S. Galasso, *Structure, Properties and Preparation of Perovskite-Type Compounds*, vol. 5 of *International Series in Monographs in Solid State Physics*. Oxford: Pergamon Press, 1969.
6. H. Katzke, P. Tolédano, and W. Depmeier, "Phase transitions between polytypes and intralayer superstructures in transition metal dichalcogenides," *Phys. Rev. B*, vol. 69, p. 134111, 2004.
7. D. P. Varn and J. P. Crutchfield, "Chaotic crystallography: How the physics of information reveals structural order in materials," *Curr. Opin. Chem. Eng.*, vol. 7, pp. 47–56, 2015.
8. G. C. Trigunayat, "A survey of the phenomenon of polytypism in crystals," *Solid State Ionics*, vol. 48, no. 1/2, pp. 3–70, 1991.
9. J. P. Hirth and J. Lothe, *Theory of Dislocations*. New York: McGraw-Hill, 2 ed., 1968.
10. D. Hull and D. J. Bacon, *Introduction to Dislocations*. New York: Butterworth-Heinemann, fifth ed., 2011.
11. T. L. Malkin, B. J. Murray, A. V. Brukhno, J. Anwar, and C. G. Salzmann, "Structure of ice crystallized from supercooled water," *Proceedings of the National Academy of Sciences of the United States of America*, vol. 109, no. 4, pp. 1041–1045, 2012.
12. D. P. Varn and J. P. Crutchfield, "Graphical representations of stacking structure in disordered layered materials," 2015. manuscript in preparation.
13. P. Caroff, J. Bolinsson, and J. Johansson, "Crystal phases in III-V nanowires: From random toward engineered polytypism," *IEEE Journal of Selected Topics in Quantum Electronics*, vol. 17, pp. 829–846, 2011.
14. D. Pan, S. Wang, B. Zhao, M. Wu, H. Zhang, Y. Wang, and Z. Jiao, "Li storage properties of disordered graphene nanosheets," *Chemistry of Materials*, vol. 21, no. 14, pp. 3136–3142, 2009.
15. E. G. Seebauer and K. W. Noh, "Trends in semiconductor defect engineering at the nanoscale," *Mater. Sci. Eng. R*, vol. 70, pp. 151–168, 2010.
16. T. R. Welberry, "One hundred years of diffuse x-ray scattering," *Metallurgical and Materials Transactions A*, vol. 45, pp. 75–84, 2014.
17. N. W. Ashcroft and N. D. Mermin, *Solid State Physics*. New York: Saunders College Publishing, 1976.
18. C. Giacovazzo, H. L. Monaco, G. Artioli, D. Viterbo, M. Milanesio, G. Ferraris, G. Gilli, P. Gilli, G. Zanotti, and M. Catti, *Fundamentals of Crystallography*, vol. 15 of *IUCr Texts on Crystallography*. Oxford University Press, 3 ed., 2011.
19. B. E. Warren, *X-Ray Diffraction*. Addison-Wesley, 1969.

20. A. Guinier, *X-Ray Diffraction in Crystals, Imperfect Crystals, and Amorphous Bodies*. New York: W. H. Freeman and Company, 1963.
21. A. L. Mackay, "Generalized crystallography," *Computers & Mathematics with Applications*, vol. B12, no. 1/2, pp. 21–37, 1986.
22. J. H. E. Cartwright and A. L. Mackay, "Beyond crystals: The dialectic of materials and information," *Phil. Trans. R. Soc. A*, vol. 370, pp. 2807–2822, 2012.
23. P. Ball, "Material Witness: Beyond the crystal," *Nat. Mater.*, vol. 13, p. 1003, 2014.
24. T. M. Cover and J. A. Thomas, *Elements of Information Theory*. Hoboken: John Wiley & Sons, second ed., 2006.
25. A. Paz, *Introduction to Probabilistic Automata*. New York: Academic Press, 1971.
26. J. E. Hopcroft and J. D. Ullman, *Introduction to Automata Theory, Languages, and Computation*. Reading: Addison-Wesley, 1979.
27. S. H. Strogatz, *Nonlinear Dynamics and Chaos: With Applications to Physics, Biology, Chemistry, and Engineering*. Westview Press, 2001.
28. J. P. Crutchfield, "Between order and chaos," *Nat. Phys.*, vol. 8, pp. 17–24, 2012.
29. J. P. Crutchfield and K. Young, "Inferring statistical complexity," *Phys. Rev. Lett.*, vol. 63, pp. 105–108, 1989.
30. D. P. Varn, G. S. Canright, and J. P. Crutchfield, "Discovering planar disorder in close-packed structures from X-ray diffraction: Beyond the fault model," *Phys. Rev. B*, vol. 66, p. 174110, 2002.
31. L. R. Rabiner, "A tutorial on hidden Markov models and selected applications," *IEEE Proc.*, vol. 77, p. 257, 1989.
32. R. J. Elliot, L. Aggoun, and J. B. Moore, *Hidden Markov Models: Estimation and Control*, vol. 29 of *Applications of Mathematics*. New York: Springer, 1995.
33. M. M. J. Treacy, J. M. Newsam, and M. W. Deem, "A general recursion method for calculating diffracted intensities from crystals containing planar faults," *Proc. R. Soc. London, Ser. A*, vol. 433, pp. 499–520, 1991.
34. E. Estevez-Rams, A. P. Madrigal, P. Scardi, and M. Leoni, "Powder diffraction characterization of stacking disorder," *Z. Kristallogr. Suppl.*, vol. 26, pp. 99–104, 2007.
35. L. Landau, "The scattering of X-rays by crystals with a variable lamellar structure," *Phys. Z. Sowjetunion*, vol. 12, p. 579, 1937.
36. I. M. Lifschitz, "On the theory of scattering of X-rays by crystals of variable structure," *Phys. Z. Sowjetunion*, vol. 12, p. 623, 1937.
37. S. Hendricks and E. Teller, "X-ray interference in partially ordered layer lattices," *J. Chem. Phys.*, vol. 10, pp. 147–167, 1942.
38. A. J. C. Wilson, "Imperfection in the structure of cobalt II. Mathematical treatment of the proposed structure," *Proc. R. Soc. Ser. A*, vol. 180, pp. 277–285, 1942.
39. H. Jagodzinski, "Eindimensionale fehlordnung in kristallen und ihr einfluss auf die röntgeninterferenzen. I. Berechnung des fehlordnungsgrades aus den röntgenintensitäten," *Acta Crystallogr.*, vol. 2, pp. 201–207, 1949.
40. H. Jagodzinski, "Eindimensionale fehlordnung in kristallen und ihr einfluss auf die röntgeninterferenzen. II. Berechnung der fehlgeordneten dichtesten kugelpackungen mit wechselwirkungen der reichweite 3," *Acta Crystallogr.*, vol. 2, pp. 208–214, 1949.
41. R. Berliner and S. Werner, "Effects of stacking faults on diffraction: The structure of lithium metal," *Phys. Rev. B*, vol. 34, pp. 3586–3603, 1986.
42. S. V. Cherepanova, "X-ray scattering on one-dimensional disordered structures," *J. Struct. Chem.*, vol. 53, pp. S109–S132, 2012.
43. D. P. Varn, G. S. Canright, and J. P. Crutchfield, "Inferring planar disorder in close-packed structures *via* ϵ-machine spectral reconstruction theory: Examples from simulated diffraction spectra," *Acta Crystallogr. A*, vol. 69, pp. 413–426, 2013.
44. B. Weiss, "Subshifts of finite type and sofic systems," *Monastsh. Math.*, vol. 77, p. 462, 1973.
45. R. Badii and A. Politi, *Complexity: Hierarchical Structures and Scaling in Physics*, vol. 6 of *Cambridge Nonlinear Science Series*. Cambridge University Press, 1997.
46. C. J. Ellison, J. R. Mahoney, and J. P. Crutchfield, "Prediction, retrodiction, and the amount of information stored in the present," *J. Stat. Phys.*, vol. 136, pp. 1005–1034, 2009.

47. J. P. Crutchfield, "The calculi of emergence: Computation, dynamics, and induction," *Physica D*, vol. 75, pp. 11–54, 1994.
48. J. P. Crutchfield and S. Marzen, "Signatures of infinity: Nonergodicity and resource scaling in prediction, complexity, and learning," *Phys. Rev. E*, vol. 91, p. 050106(R), 2015.
49. A. L. Ortiz, F. Sánchez-Bajo, F. L. Cumbrera, and F. Guiberteau, "The prolific polytypism of silicon carbide," *J. Appl. Crystallogr.*, vol. 46, pp. 242–247, 2013.
50. D. P. Varn, G. S. Canright, and J. P. Crutchfield, "Inferring planar disorder in close-packed structures *via* ϵ-machine spectral reconstruction theory: Structure and intrinsic computation in zinc sulfide," *Acta Crystallogr. B*, vol. 63, pp. 169–182, 2007.
51. D. P. Varn, G. S. Canright, and J. P. Crutchfield, "ϵ-Machine spectral reconstruction theory: A direct method for inferring planar disorder and structure from X-ray diffraction studies," *Acta Crystallogr. A*, vol. 69, pp. 197–206, 2013.
52. H. Kantz and T. Schreiber, *Nonlinear Time Series Analysis*. Cambridge: Cambridge University Press, 2 ed., 2004.
53. B. I. Nikolin and A. Y. Babkevich, "A Monte Carlo simulation of random stacking faults in close-packed structures," *Acta Crystallogr. A*, vol. 45, pp. 797–801, 1989.
54. D. A. Keen and R. L. McGreevy, "Structural modelling of glasses using reverse Monte Carlo simulation," *Nature*, vol. 344, pp. 423–425, 1990.
55. T. M. Michels-Clark, V. E. Lynch, C. M. Hoffmann, J. Hauser, T. Weber, R. Harrison, and H. B. Bürgi, "Analyzing diffuse scattering with supercomputers," *J. Appl. Crystallogr.*, vol. 46, pp. 1616–1625, 2013.
56. D. P. Varn and J. P. Crutchfield, "From finite to infinite range order via annealing: The causal architecture of deformation faulting in annealed close-packed crystals," *Phys. Lett. A*, vol. 324, no. 4, pp. 299–307, 2004.
57. R. G. James, J. R. Mahoney, C. J. Ellison, and J. P. Crutchfield, "Many roads to synchrony: Natural time scales and their algorithms," *Phys. Rev. E*, vol. 89, p. 042135, 2014.
58. G. Ferraris, E. Makovicky, and S. Merlino, *Crystallography of Modular Materials*, vol. 15. Oxford University Press, 2008.
59. D. P. Varn and G. S. Canright, "The crystal problem for polytypes," *Acta Crystallogr. A*, vol. 57, pp. 4–19, 2001.
60. P. M. Riechers, D. P. Varn, and J. P. Crutchfield, "Pairwise correlations for layered close-packed structures," *Acta Crystallogr. A*, vol. 71, p. In press, 2015.
61. U. Grimm, "Aperiodic crystals and beyond," *Acta Crystallogr. B*, vol. 71, pp. 258–274, 2015.
62. F. Axel and H. Terauchi, "High-resolution X-ray-diffraction spectra of Thue-Morse GaAs-AlAs heterostructures: Towards a novel description of disorder," *Phys. Rev. Lett.*, vol. 66, pp. 2223–2226, 1991.
63. V. K. Kabra and D. Pandey, "Long-range ordered phases without short-range correlations," *Phys. Rev. Lett.*, vol. 61, pp. 1493–1496, 1988.
64. J. Yeomans, "The theory and application of axial Ising models," *Solid State Physics*, vol. 41, pp. 151–200, 1988.
65. J. Yi and G. S. Canright, "Possible disordered ground states for layered solids and their diffraction patterns," *Phys. Rev. B*, vol. 53, pp. 5198–5210, 1996.
66. E. Estevez-Rams, B. Aragon-Fernandez, H. Fuess, and A. Penton-Madrigal, "Diffraction patterns of stacked layer crystals," *Phys. Rev. B*, vol. 68, p. 064111, 2003.
67. P. M. Riechers and J. P. Crutchfield, "Spectral decomposition of structural complexity: Meromorphic functional calculus of nondiagonalizable dynamics," 2014. manuscript in preparation.
68. A. V. Oppenheim and R. W. Schafer, *Digital Signal Processing*. Englewood Cliffs: Prentice-Hall, 1975.
69. E. Estevez-Rams, U. Welzel, A. P. Madrigal, and E. J. Mittemeijer, "Stacking and twin faults in close-packed crystal structures: Exact description of random faulting statistics for the full range of faulting probabilities," *Acta Crystallogr. A*, vol. 64, pp. 537–548, 2008.
70. J. W. Sun, T. Robert, A. Andreadou, A. Mantzari, V. Jokubavicius, R. Yakimova, J. Camassel, S. Juillaguet, E. K. Polychroniadis, and M. Syväjärvi, "Shockley-Frank stacking faults in 6H-SiC," *J. Appl. Phys.*, vol. 111, p. 113527, 2012.
71. J. P. Crutchfield, C. J. Ellison, and P. M. Riechers, "Exact complexity: The spectral decomposition of intrinsic computation," *Santa Fe Institute Working Paper 2013-09-028*, 2013.